Reply to reviewers (responses are *italicized*)

1. Reply to SC C5922:

Thanks a lot for your kindly comment. We revised the sentence as follows:

"Photomineralization alone or combined with photochemically stimulated biomineralization has been suggested as a significant sink of DOC in many rivers and lakes (e.g. Bertilsson and Tranvik, 2000; Vähätalo and Wetzel, 2004; Cory et al., 2014) and a major sink of terrigenous DOC in coastal and shelf waters (Miller and Zepp, 1995; Aarnos et al., 2012; Fichot and Benner, 2014)."

2. Reply to Reviewer #1 (RC C6270)

We thank the reviewer very much for his/her encouragement and positive opinions on our work. Our responses are italicized.

General comments

1) The DOC loss could partially be due to CO photoproduction yet this was not discussed. I think the authors need to correct their estimates (or provide bounds) considering some loss as CO.

We added the following text at the beginning of Section 3.2 for clarification: "Note that photochemical DOC loss leads to production of CO_2 (in the form of dissolved inorganic carbon, DIC) and carbon monoxide (CO), with DIC being the main product (Miller and Zepp, 1995). As photomineralization rates reported in this study were equated to DOC loss rates, the former also included the CO component. Based on our unpublished AQY spectrum for CO photoproduction from CDOM in Saguenay River surface water ($AQY_{CO}(\lambda) = 3.07 \times 10^{-10} \exp(5661 / (149.1 + \lambda)$, where λ is wavelength in nanometers), we estimated that the ratio of DIC to CO photoproduction was 31. Photomineralization was thus overwhelmingly dominated by DIC production in our study."

2) p14312 L12: Might it be better to just describe this as an oxygen gradient (supersaturated, saturated, depleted) after describing how the oxygen conditions were achieved. I know there is the problem of some reoxygenation during sample transfer and I think the authors do a good job of making that caveat clear, but reference to O2-, air-, N2-purging is cumbersome.

"O2-saturated" and "O2-supersaturated" are a bit confusing when they refer to [O2] at equilibrium with air and close to saturation with pure O2, respectively, since "O2-saturated" is usually understood as "saturated with pure O2", and "supersaturated" can cover wide, unspecified ranges. Although the [O2]s in the O2- and N2-purged samples somewhat deviated from those expected from equilibrium

with O2 and N2, respectively, they in fact are close to the equilibrium concentrations. For simplicity and approaching conformity to the practice of previous studies (Gao and Zepp, 1998; Xie et al., 2004; Lou and Xie, 2006), we now refer to the air-, O2-, and N2-purging as air-, O2-, and N2-treatment, respectively. As we have reported the initial [O2]s for each of these treatments and explicitly stated that the [O2] for "O2-saturated" was slightly below O2-saturation and for "N2-saturated" was slightly above free of O2, we hope there will be no confusion/misunderstanding arises from using these expressions.

3) P14313: "TDOM" often is used for terrigenous (terrestrial) DOM so its use to describe transparent CDOM is confusing. Also, perhaps misleading. For example, is this meant to convey transparency at 330 nm or transparency at all wavelenghts, even deep into the UV? If the former, this certainly is not correct as molecules may lack charge transfer for absortpion bands in the mid UV but absorb strongly at say 254 nm. If the latter, the discussion as written was purely speculative. One way forward is to perhaps show how slope values (S or SR) change during photodegradation. If slope changes all line up together over the first 50 hours of exposure (re: Fig 3) and then diverge, you may get a bit more insight to the differences between oxygen conditions.

We agree with the reviewer. We tested other wavelengths, 254 nm, 300 nm, and 400 nm, and found the ratios of the fractional DOC loss to the fractional a_{CDOM} loss are somewhat lower compared to those at 330 nm but the patterns are similar (Fig. 1 below). The discussion of TDOM is now removed and replaced with a statement of "A closer examination of the data indicates that the ratio of the fractional DOC loss to the fractional $a_{CDOM}(330)$ loss decreased from 0.82 in the N_2 treatment to 0.64 in the air treatment to 0.54 in the O_2 treatment (Fig. 5C). Similar results were obtained at the wavelengths of 254 nm, 300 nm, and 400 nm (data not shown). Therefore, photochemical DOC loss proceeded more efficiently under O_2-deficiency than under oxic conditions on a per-a_{CDOM}-loss basis, opposite to the trend of the time-based DOC loss rate. In other words, higher fractions of CDOM were mineralized under O_2-depletion than under oxygenation."

Accordingly, the original statement in the Summary, "Photochemical breakdown of CDOM led to a nearly complete mineralization (i.e. DIC production) under suboxic conditions but to only a partial mineralization under oxic conditions, with the rest transformed to TDOM", is modified to "Photochemical breakdown of CDOM led to a higher degree of mineralization (i.e. DIC production) under suboxic conditions than under oxic conditions".

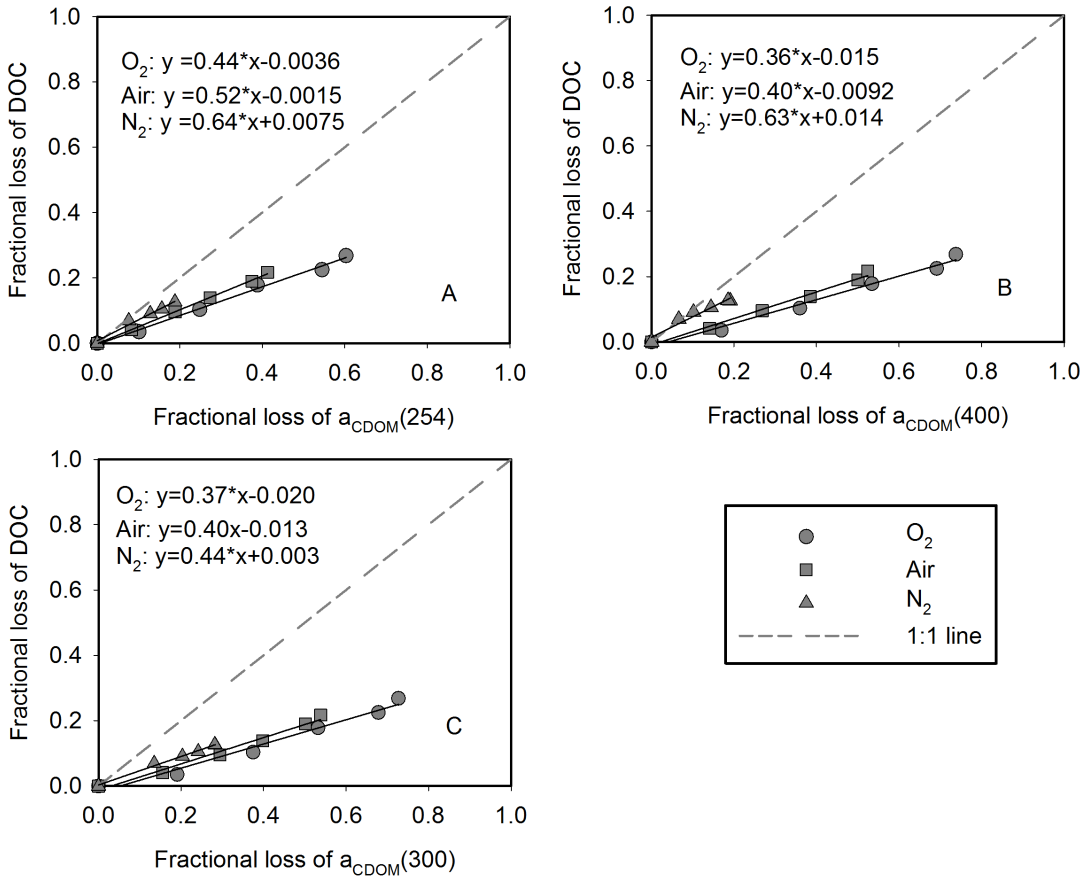

Fig. 1. Fractional DOC loss versus fractional a_{CDOM} loss at 254 nm (A), 300 nm (B), and 400 nm (C).

Following the reviewer's suggestion, we also plotted the time-course variations of the spectral slope ratio (now Fig. 3C), S_R, defined as the slope coefficient between 275-295 nm divided by the slope coefficient between 350-400 nm (Helms et al., 2008). A short discussion of S_R was added to Section 3.1, which is copied as follows:

At the start of this section: "Figure 3 shows the time-course variations of [O_2], pH, the absorption coefficient at 330 nm ($a_{CDOM}(330)$), and the spectral slope ratio (S_R) defined as the ratio of the spectral slope coefficient between 275 nm and 295 nm to that between 350 nm and 400 nm. S_R has been used to characterize the source, molecular size, and photoprocessing of CDOM (Helms et al., 2008)."
After describing loss of CDOM: "S_R continuously increased over the entire irradiation period in the air- and O_2-treatments; S_R in the N_2-treatment increased with irradiation time up to ~120 h and became stable thereafter (Fig. 3C), suggesting a complete exhaustion of O_2. Notably, the changes in S_R for the three different O_2 levels nearly lined up together during the first 24 h of irradiation but started diverging at ~48 h when [O_2] in the N_2-treatment dropped to a constant level (Fig. 3A)."

4) The role of lignin in explaining these results could be better emphasized. The methoxy (-OCH3) groups in dissolved lignin are good candidates for CO, CO2, and

CH4. P14314, L17-21: Makes sense if the aldehydes in lignin are being oxidized to acids.

We are unable to find papers directly linking the methoxy groups in dissolved lignin to CO2 photoproduction or photochemical DOC loss. Benner and Kaiser (2011) revealed that the photodegradation rate constant of lignin phenols increases with the number of methoxy substitutions on the aryl ring. However, as the lignin and its degradation only account for minor portions of the bulk DOC and the photochemical DOC loss, respectively, the results of Benner and Kaiser (2011) do not prove that the methoxy groups play a critical role in DOC photodegradation or that they are good candidates for CO2 photochemically produced.

Methoxy groups do enhance the efficiency of CO photoproduction from model aromatic compounds (Stubbins et al., 2008). Nevertheless, the direct precursors for CO are likely other compounds, such as formaldehyde, that are produced from photodegradation of methoxy-substituted aromatic compounds (Stubbins et al., 2008). Furthermore, the CO AQY rapidly decreases with photobleaching (Zhang et al., 2006), suggesting a quick photochemical removal of the methoxy-substituted lignin phenols if they do play a dominant role in CO photoproduction. In contrast, the DOC photomineralization AQY observed in the present study either remained stable (in the O_2-saturated sample) or increased (in the O_2-supersaturated sample) with photobleaching, which appears contradictory with a methoxy-driven mechanism.

CH_4 production from photodegradation of methoxy-substituted lignin model compounds, such as methoxy-substituted stilbenes, under anaerobic conditions has been reported (e.g. Weir et al., 1995; 1996). The proposed mechanism involves the cleavage of the O-CH_3 bond, producing the CH_3 radical followed by H-abstraction to generate CH_4. A brief discussion of this CH_4 production pathway, as shown below, is now added to "Future work" in Section 4:
"…and methyl ester that are naturally present in aquatic environments. For river and riverine-impacted coastal waters, particular attention should be paid to methoxy-substituted phenols in dissolved lignin, since these compounds are highly susceptible to photodegradation (Benner and Kaiser, 2011) and since the methoxy groups in certain lignin model phenols have been demonstrated to be efficient precursors of CH_4 under anaerobic conditions (Weir et al., 1995). Moreover, anoxic microniches…"

5) The CH3 radical may be a key intermediate in low O2 settings. I wondered, too, if nitrate photolysis is important in these photochemical pathways?

Photolysis of nitrate produces OH radicals (Zarifiou and True, 1979). The reactions of the OH radical with bromide and carbonate/bicarbonate produce the Br_2^- and CO_3^- radicals (Zehavi and Rabani, 1972; True and Zafiriou, 1987), which might be involved in the photosensitized production of the CH_3 radical and hence CH_4 (Bange

and Uher, 2005). However, this process can be important only in waters containing elevated nitrate concentrations. In waters having normal levels of nitrate, the dominant source of the OH radical is CDOM photooxidation (Mopper and Zhou, 1990). This topic is beyond the scope of the present paper (due to lack of relevant data, such as nitrate concentrations) but certainly warrants investigation in the future.

Specific comments

p14310, L8: "moisturized" – better word choice here; not worried about methane's complexion! :)

The sentence is revised to "…, the dry CH_4 standard was saturated with water vapor before injection."

p14315, L15: "different" not "differed"

"differed" is changed to "different".

p14321, L9: This result has been observed in CDOM photobleaching; may wish to explore this result a bit more. Photomethanificiation tracks more closely with photobleaching than does photooxidation? Perhaps photomethanification is more of a primary photochemical process. No photodecarboxylation requried, for example.

In this study, photomethanification in the air-treatment tracked nicely with both photobleaching (Fig. 6B) and photomineralization (i.e. a major photooxidation pathway, Fig. 5C). This was because photobleaching and photomineralization were correlated very well (Fig. 5B). The relative contributions of UVB (16%), UVA (44%), VIS (40%) to CH_4 photoproduction were also similar to those (UVB: 15%; UVA: 41%; VIS: 44%) for photomineralization. Therefore, based on these results, it's hard to infer whether photomethanification is a primary or secondary photochemical process. Bange and Uher (2005), however, found that photoproduction of CH_4 from acetone is a photosensitized process (CH_4 is produced in the presence of CDOM but not produced in pure water). The observed behavior of CH_4 production at different O_2 levels, is in line with the mechanism of the CH_3 radical as an intermediate followed by H-abstraction, as proposed by Bange and Uher (2005). The reaction of the CH_3 radical with O_2 is favored under oxic conditions, leading to lower CH_4 production rates. This mechanism has already been discussed in our paper.

For these reasons, we decided not to further elaborate the mechanism but added a line to the Summary and Future Work that future work should also elucidate the mechanisms of photomethanification of organic matter in natural waters.

References:

Aarnos, H., Ylöstalo, P., and Vähätalo, A. V.: Seasonal phototransformation of

dissolved organic matter to ammonium, dissolved inorganic carbon, and labile substrates supporting bacterial biomass across the Baltic Sea, J. Geophys. Res., 117, G01004, doi: 10.1029/2010JG001633, 2012.

Bange, H. W. and Uher, G.: Photochemical production of methane in natural waters: implications for its present and past oceanic source, Chemosphere, 58, 177–183, 2005.

Benner, R. and Kaiser, K.: Biological and photochemical transformations of amino acids and lignin phenols in riverine dissolved organic matter, Biogeochemistry, 102, 209–222, doi:10.1007/s10533-010-9435-4, 2011.

Bertilsson, S. and Tranvik, L. J.: Photochemical transformation of dissolved organic matter in lakes, Limnol. Oceanogr., 45, 753–762, doi: 10.4319/lo.2000.45.4.0753, 2000.

Cory, R. M., Ward, C. P., Crump, B. C., and King, G. W.: Sunlight controls water column processing of carbon in arctic fresh waters, Science, 345, doi:10.1126/science.1253119, 2014.

Fichot, C. G. and Benner, R.: The fate of terrigenous dissolved organic carbon in a river-influenced ocean margin, Global Biogeochem. Cy., 28, 1–19, doi: 10.1002/2013GB004670, 2014.

Gao, H., Zepp, R. G.: actors influencing photoreactions of dissolved organic matter in a coastal river of the southeastern United States, Environ. Sci. Technol., 32, 2940–2946, 1998.

Helms, J. R., Stubbins, A., Ritchie, J. D., Minor E. C., Kieber, D. J., and Mopper, K. : Absorption spectral slopes and slope ratios as indicators of molecular weight, source, and photobleaching of chormophoric dissolved organic matter, Limnol. Oceanogr., 53 (3), 955–969, 2008.

Lou, T., Xie, H.: Photochemical alteration of the molecular weight of dissolved organic matter, Chemosphere, 65, 2333–2342, 2006.

Miller, W. L. and Zepp, R. G.: Photochemical production of dissolved inorganic carbon from terrestrial organic matter: significance to the oceanic organic carbon cycle, Geophys. Res. Lett., 22, 417–420, 1995.

Mopper, K. and Zhou, X. L.: Hydroxyl radical photoproduction in the sea and its potential impact on marine processes, Science, 250, 661–664, 10.1126/science.250.4981.661, 1990.

Stubbins, A., Hubbard, V., Uher, G., Law, C. S., Upstill-Goddard, R. C., Aiken, G. R., and Mopper, K.: Relating carbon monoxide photoproduction to dissolved organic

matter functionality, Environ. Sci. Technol., 42, 3271–3276, 2008.

True, M. B. and Zafiriou, O. C.: Reaction of Br_2^- produced by flash photolysis of seawater with components of the dissolved carbonate system, in: Photochemistry of Environmental Aquatic Systems, edited by: Zika, R. G. and Cooper, W. J., American Chemical Society, Washington, DC, USA, 106–115, 1987.

Vähätalo, A. V. and Wetzel, R. G.: Photochemical and microbial decomposition of chromophoric dissolved organic matter during long (months–years) exposures, Mar. Chem., 89, 313–326, doi:10.1016/j.marchem.2004.03.010, 2004.

Weir, N. A., Arct, J., and Ceccarelli, A.: Photodegradation of lignin model compounds: part 2—substituted stilbenes, Polymer Degradation and Stability, 47, 289–297, 1995.

Weir, N. A., Arct, J., Ceccarelli, A., and Puumala, D.: Long-wave photochemistry of di-methoxylated compounds related to lignin, Polymer Degradation and Stability, 52, 119-129, 1996.

Xie, H., Zafiriou, O. C., Cai, W.-J., Zepp, R. G., Wang, Y.: Photooxidation and its effects on the carboxyl content of dissolved organic matter in two coastal rivers in the southeastern United States, Environ. Sci. Technol., 38, 4113–4119, 2004.

Zafiriou, O. C. and True, M. B.: Nitrate photolysis in seawater by sunlight, Mar. Chem., 8, 33–42, doi:10.1016/0304-4203(79)90030-6, 1979.

Zehavi, D. and Rabani, J.: The oxidation of aqueous bromide ions by hydroxyl radicals. A pulse radiolytic investigation, J. Phys. Chem., 76, 312–319, 1972.

Zhang, Y., Xie, H. X. and Chen, G. H.: Factors affecting the efficiency of carbon monoxide photoproduction in the St. Lawrence estuarine system (Canada), Environ. Sci. Technol., 40, 7771-7777, 2006.

3. Reply to Reviewer #2 (RC C6635)

We greatly appreciate the reviewer's favorable comments on our study. Our responses are italicized.

The investigation of DMS as a precursor to methane photoproduction is interesting and it would be nice in future work to also look at O-methylated phenolic compounds found in lignin. My only minor comment is that the authors don't discuss the scale of carbon monoxide photoproduction in the context of DOC photomineralisation, it would be helpful to get some idea of how much carbon could be diverted to CO if the authors have measurements from Saguenay River/St. Laurence Estuary.

Reviewer #1 also commented on these two issues (precursors of CH_4 in lignin and CO photoproduction). Please see our responses to Reviewer #1's first and fourth general comments.

Photomineralization and photomethanification of dissolved organic matter in Saguenay River surface water (marked-up in blue color)

Y. Zhang[1, 2], H. Xie[2]

[1]Key Laboratory of Coastal Environmental Processes and Ecological Remediation, Yantai Institute of Coastal Zone Research, Chinese Academy of Sciences, Yantai, Shandong Province 264003, P. R. China

[2]Institut des sciences de la mer de Rimouski, Université du Québec à Rimouski, Rimouski, Québec G5L 3A1, Canada

Correspondence to: H. Xie (huixiang_xie@uqar.ca)

Abstract. Rates and apparent quantum yields of photomineralization (AQY_{DOC}) and photomethanification (AQY_{CH4}) of chromophoric dissolved organic matter (CDOM) in Saguenay River surface water were determined at three widely differing dissolved oxygen concentrations ($[O_2]$) (suboxic, air-saturation, and oxygenated) using simulated-solar radiation. Photomineralization increased linearly with CDOM absorbance photobleaching for all three O_2 treatments. Whereas the rate of photochemical dissolved organic carbon (DOC) loss increased with increasing $[O_2]$, the ratio of fractional DOC loss to fractional absorbance loss showed an inverse trend. CDOM photodegradation led to a nearly complete mineralization under suboxic conditions but to only a partial mineralization under oxic conditions. AQY_{DOC} determined under oxygenated, suboxic, and air-saturated conditions increased, decreased, and remained largely constant with photobleaching, respectively; AQY_{DOC} obtained under air-saturation with short-term irradiations could thus be applied to longer exposures. AQY_{DOC} decreased successively from ultraviolet B (UVB) to ultraviolet A (UVA) to visible (VIS), which, alongside the solar irradiance spectrum, points to VIS and UVA being the primary drivers for photomineralization in the water column. The photomineralization rate in the Saguenay River was estimated to be 2.31×10^8 mol C yr^{-1}, accounting for only 1% of the annual DOC input into this system.

Photoproduction of CH_4 occurred under both suboxic and oxic conditions and increased with decreasing $[O_2]$, with the rate under suboxic conditions ~7-8 times that under oxic conditions. Photoproduction of CH_4 under oxic conditions increased linearly with photomineralization and photobleaching. Under air-saturation, 0.00057% of the photochemical DOC loss was diverted to CH_4, giving a photochemical CH_4 production rate of 4.36×10^{-6} mol m^{-2} yr^{-1} in the Saguenay River and, by extrapolation, of $(1.9–8.1) \times 10^8$ mol yr^{-1} in the global ocean. AQY_{CH4} changed little

311 with photobleaching under air-saturation but increased exponentially under suboxic
312 conditions. Spectrally, AQY_{CH4} decreased sequentially from UVB to UVA to VIS,
313 with UVB being more efficient under suboxic conditions than under oxic conditions.
314 On a depth-integrated basis, VIS prevailed over UVB in controlling CH_4
315 photoproduction under air-saturation while the opposite held true under O_2-deficiency.
316 An addition of micromolar levels of dissolved dimethyl sulfide (DMS) substantially
317 increased CH_4 photoproduction, particularly under O_2-deficiency; DMS at nanomolar
318 ambient concentrations in surface oceans is, however, unlikely a significant CH_4
319 precursor. Results from this study suggest that CDOM-based CH_4 photoproduction
320 only marginally contributes to the CH_4 supersaturation in modern surface oceans and
321 to both the modern and Archean atmospheric CH_4 budgets, but that the photochemical
322 term can be comparable to microbial CH_4 oxidation in modern oxic oceans. Our
323 results also suggest that anoxic microniches in particulate organic matter and
324 phytoplankton cells containing elevated concentrations of precursors of the methyl
325 radical such as DMS may provide potential hotspots for CH_4 photoproduction.

326

327 **1. Introduction**

328 Solar radiation in the ultraviolet (UV) and visible (VIS) regimes can break down
329 chromophoric dissolved organic matter (CDOM), leading to the loss of absorbance
330 (i.e. photobleaching) (Del Vecchio and Blough, 2002) and dissolved organic carbon
331 (DOC, i.e. photomineralization) (Obernosterer and Benner, 2004) and the production
332 of CO_2 (Miller and Zepp, 1995), biolabile carbon (Kieber et al., 1989; Miller et al.
333 2002), and various biologically and atmospherically active trace compounds (Moran

and Zepp, 1997; Liss et al., 2014). Photomineralization alone or combined with photochemically stimulated biomineralization has been suggested as a significant sink of DOC in many rivers and lakes (e.g. Bertilsson and Tranvik, 2000; Vähätalo and Wetzel, 2004; Cory et al., 2014) and a major sink of terrigenous DOC in coastal and shelf waters (Miller and Zepp, 1995; Aarnos et al., 2012; Fichot and Benner, 2014). Many trace gases produced from CDOM-involved photoprocesses are supersaturated in natural waters (e.g. carbonyl sulfide, iodomethane, carbon monoxide), thereby contributing to their budgets in the atmosphere (Liss et al., 2014). CDOM photochemistry therefore plays an important role in biogeochemical cycling of DOC and trace gases in natural waters (Mopper and Kieber, 2002; Zafiriou, 2002).

Methane (CH_4), the second most important greenhouse gas, is one of the trace gaseous compounds known to emit from aquatic systems to the atmosphere (Cicerone and Oremland, 1988; IPCC, 2013). Although CH_4 in natural waters has long been thought to be produced exclusively under anaerobic conditions (Reeburgh, 2007), recent studies have revealed that aerobic microbial metabolism can also generate CH_4 through decomposition of methylated precursors, such as methylphosphonates (Karl et al., 2008; Metcalf et al., 2012). More recently, a number of studies observed correlations between CH_4 concentration and concentrations of dimethylsulfoniopropionate (DMSP) and/or dimethylsulfoxide (DMSO) in the Arctic and Pacific Oceans (Damm et al., 2008, 2015; Weller et al., 2013; Zindler et al., 2013). Carbon isotope tracer experiments also confirmed DMSP and its degradation product, dimethylsulfide (DMS), to be plausible substrates of methylotrophic microbes leading to CH_4 production in surface seawater (Damm et al., 2010; Florez-Leiva et al., 2013). In addition to biomethanation, abiotic processes have also been suggested as potential

358 CH_4 production pathways in oxygenated natural waters. Tilbrook and Karl (1995)
359 observed formation of CH_4 from sediment trap-collected sinking particles after
360 exposure to solar radiation and suspected a photochemical source. Bange and Uher
361 (2005) assessed the possibility of CH_4 photoproduction (i.e. photomethanification)
362 from CDOM in a number of river and estuarine systems and concluded that this
363 pathway is significant only under anoxia in the presence of an added methyl radical
364 precursor. They only tested acetone but suggested that other water-soluble methyl
365 radical precursors such as acetonitrile, methionine, and dimethyl sulfide (DMSO),
366 could be good candidates as well.

367 The purpose of this study is to explore the role of photochemistry in the cycling
368 of DOC and CH_4 in the highly colored surface water of the Saguenay River on the
369 north shore of the St. Lawrence estuary (Canada). We determined the apparent
370 quantum yields (AQYs) of photomineralization and photomethanification of CDOM
371 and examined the effects of dissolved oxygen (O_2) and the dose and spectral
372 composition of incident light on these two photoprocesses. Given the recent finding of
373 the involvement of DMS in microbial CH_4 production (Florez-Leiva et al., 2013), we
374 also investigated this compound as a potential precursor of CH_4 photochemically
375 produced.

376

377 **2. Experimental Section**

378 **2.1. Study site and sample collection**

379 The Saguenay River (Fig. 1), extending 165 km long from Lac Saint-Jean to
380 Tadoussac and having a mean discharge of 1194 m^3 s^{-1} (Bélanger, 2003), is the
381 principal tributary of the St. Lawrence estuary. Seasonal variations in both discharge

382 rate and water quality tend to be equalized due to regulation by hydropower dams in
383 the upper reach of the river (Schafer et al., 1990; Roy et al., 2000). The Saguenay
384 River intersects the St. Lawrence estuary near Tadoussac, where tides can propagate
385 upriver to ~15 km upstream of Chicoutimi. About 15 km downstream of Chicoutimi
386 lies the Saguenay Fjord, which is characterized by a strong vertical stratification with
387 a thin surface mixed layer of 5–20 m in summer (Drainville, 1968) and a thinner layer
388 in winter (Bourgault et al., 2012). Terrigenous humic substance is the dominant
389 component (over 50% in terms of DOC) of dissolved organic matter in the surface
390 water of the fjord (Tremblay and Gagné, 2009) and CDOM behaves conservatively in
391 the entire water column (Xie et al., 2012).

392 Surface water was taken at Chicoutimi (48.4°N, 71.1°W) at ebb tide on 20
393 November 2013 using a clean high-density polyethylene bucket, transferred into 20-L
394 acid-washed, collapsible polyethylene bags (Cole-Parmer), and immediately brought
395 back to the laboratory in Rimouski. The water was gravity-filtered through Whatman®
396 Polycap 75 AS filtration capsules sequentially containing 0.2 μm glass microfiber and
397 Nylon membrane filters. The capsules were extensively flushed with Nanopure water
398 and then sample water before they were used to avoid contamination. This procedure
399 removed more than 99% of bacteria as confirmed by flow cytometry with an Epics
400 Altra flow cytometer (Beckman Coulter) following the procedure reported by Xie et
401 al. (2009). Salinity was measured to be 0.1 using an YSI model 30 handheld salinity,
402 conductivity and temperature system. All samples were kept at 4^{o}C in the dark until
403 further processing.

404

405 **2.2. Irradiation**

406 Immediately before irradiation, water samples were re-filtered through 0.2 μm
407 nylon filters (Millipore) to minimize bacterial contamination. To assess the effect of
408 dissolved O_2 on the photoprocesses of interest, samples were bubbled with
409 medical-grade air, pure O_2, and pure N_2 (Air Liquide) for at least 1.5 h to obtain three
410 widely different levels of O_2. Dissolved O_2 concentrations ($[O_2]$s) were measured to
411 be 271.2 μmol L^{-1}, 1023.0 μmol L^{-1} and 53.1 μmol L^{-1} in the air-, O_2-, and N_2-purged
412 water, respectively. The $[O_2]$ in the N_2-purged water was slightly higher than expected
413 from equilibrium with pure N_2 while vice versa for the O_2-purged water due mainly to
414 exchange with the atmosphere during sample transfer. Herein the air-, O_2-, and N_2-
415 bubbling are referred to as air-, O_2-, and N_2-treatment, respectively. After bubbling,
416 water was transferred into cylindrical quartz cells (length: 25.0 cm; i.d.: 2.2 cm). The
417 cells were sealed without headspace with ground glass stoppers following sufficient
418 overflowing. The value of pH remained constant (7.22) under air-purging but
419 increased significantly under O_2- and N_2-purging. In the latter case, the pH was
420 adjusted to the initial value with 0.1 N HCl (ACS grade, BDH) to minimize potential
421 effects of pH variation on CDOM photochemistry (Anesio and Granéli, 2003; Molot
422 et al., 2005; Hong et al., 2014).

423 Irradiations were performed using a Suntest XLS+ solar simulator equipped with
424 a 1500 W xenon lamp. The sample-filled quartz cells were horizontally immersed (~2
425 mm below water surface) in a temperature-controlled water bath (20 ± 1°C) located
426 immediately beneath the exposure chamber of the solar simulator. Samples were
427 irradiated under full spectrum in time series up to 181.8 h, duplicate samples being
428 sacrificed at each time point for analysis. Photon fluxes reaching the irradiation
429 surface were determined at intervals of 1 nm using an OL-754 spectroradiometer
430 fitted with a 2-inch OL IS-270 integrating sphere calibrated with an OL 752-10E

irradiance standard (Optronics Laboratories). The solar simulator's photon fluxes in the UVB (280–320 nm), UVA (320–400 nm), and VIS (400–600 nm) were, respectively, 1.54, 0.85, and 1.25 times those of the noontime clear-sky sunlight measured in May at Rimouski (45.5°N), Canada (Fig. 2). One hundred and eighty-one point eight hours of solar-simulated irradiation thus corresponded to 19.7-d UVB, 35.7-d UVA and 24.2-d VIS irradiations with clear-sky sunlight at the latitude of 45.5°N, assuming 1-d clear-sky irradiation to be equivalent to 6-h noontime irradiation (Miller and Zepp, 1995).

Additional irradiations of N_2- and air-purged samples (in triplicate) were conducted using Mylar-D films (50% transmittance cutoff at 324 nm) and UF-4 Plexiglas sheets (50% transmittance cutoff at 408 nm) as light filters to evaluate the relative importance of UVB (full spectrum minus Mylar-D), UVA (Mylar-D minus UF-4), and VIS (UF-4) radiation in the photoprocesses examined. Irradiations underwent in a start-end mode and lasted from 48 h to 75 h, being shorter for N_2-purged samples than for air-purged samples.

To evaluate if DMS can produce CH_4 through CDOM-mediated photochemistry, the re-filtered water was amended with 20.0 μmol L^{-1} DMS (≥99.0% purity, Sigma-Aldrich) and irradiated under full spectrum in time series up to 166.3 h (in duplicate). In addition, a start-end type of irradiation (44.3 h) was carried out with samples forming a DMS concentration series of 10.0, 20.0, 50.0, and 100.0 μmol L^{-1}. The DMS tests used air- and N_2-purged samples only. All irradiated samples were accompanied with parallel dark controls which showed no significant changes in the variables measured in this study.

2.3. Analysis

CH_4 was measured using a static headspace method similar to that reported by Xie et al. (2002) for dissolved carbon monoxide measurement. Briefly, water samples were transferred to a 50 mL glass syringe, into which 5 mL CH_4-free N_2 was introduced to obtain a 1:6 gas:water ratio. The syringe was vigorously shaken for 4 min and the equilibrated headspace gas was injected into a Peak Performer 1 FID gas chromatograph (2 mL sample loop; Peak Laboratories, USA) for CH_4 quantification. The analyzer was standardized by frequent injections of a gaseous CH_4 standard of 4.8 parts per million by volume (ppmv) (balance: N_2; Air Liquide) traceable to the National Institute of Standards and Technology (NIST). Such a single-point calibration protocol was adopted since pre-study tests confirmed that the analyzer consistently responded linearly up to 10.5 ppmv. In keeping with the samples' 100% relative humidity, the dry CH_4 standard was moisturized with water before injection. To estimate the analytical blank, a water sample was repeatedly extracted with pure N_2 until its CH_4 signal diminished to a stable level. Nine times of subsequent analyses of the extracted sample arrived at a mean blank of 0.034 nmol L^{-1} with a standard deviation of 0.015 nmol L^{-1}. The lower detection limit, defined as three times the blank, was thus 0.045 nmol L^{-1}. The analytical reproducibility was determined to be ± 4% (n = 7) at a CH_4 concentration ($[CH_4]$) of ~5 nmol L^{-1}. The amount of photochemically produced CH_4 was calculated as the difference in $[CH_4]$ between the irradiated sample and the parallel dark control.

Absorbance spectra were recorded at room temperature from 600 to 280 nm at 1 nm intervals using a Perkin-Elmer lambda-35 dual beam UV-visible spectrometer fitted with 1 cm quartz cells and referenced to Nanopure water. The sample cell was rinsed with methanol, pure water, and sample water between individual scans. A

baseline correction was applied by subtracting the absorbance value averaged over 683–687 nm from all spectral values (Babin et al., 2003). The Napierian absorption coefficient of CDOM at wavelength λ, $a_{CDOM}(\lambda)$ (m^{-1}), was calculated as 2.303 times the absorbance divided by the cell's light path length in meters. The lower detection limit of the absorption coefficient measurement, defined as three times the standard deviation of five replicate analyses of pure water was 0.02 ± 0.01 m^{-1} over 280–600 nm. DOC samples were acidified to pH ~2 with 2N HCl to remove the dissolved inorganic carbon and analyzed in triplicate using a Shimadzu TOC-Vcpn carbon analyzer calibrated with potassium biphthalate. The system was checked, at intervals of seven consecutive sample analyses, against Hansell's low-carbon and deep Florida Strait (700 m) reference waters with DOC concentrations ([DOC]s) of 1 μmol L^{-1} and 41–44 μmol L^{-1}, respectively. The coefficient of variation on five replicate injections was < 1.5%. [O_2] was measured with a WTW Oxi 340 meter equipped with a CellOX 325 oxygen sensor (analytical accuracy: ± 0.5%). A Thermo Orion pH meter (model 420A) fitted with a Ross Orion combination electrode was used to determine pH; the system was standardized with three NIST buffers at pH 4.01, 7.00, and 10.01.

2.4. Calculations of absorbed photons and AQYs

The photon flux absorbed by CDOM, $Q_{CDOM}(\lambda)$ (mol photons s^{-1} nm^{-1}), was calculated according to Hu et al. (2002):

$$Q_{CDOM}(\lambda) = Q_0(\lambda) \times (a_{CDOM}(\lambda) / a_t(\lambda)) \times S \times [1 - \exp(-a_t(\lambda) \times L] \quad (1)$$

$Q_0(\lambda)$ is the photon flux reaching the water surface inside the quartz cell (mol photons m^{-2} s^{-1} nm^{-1}). The attenuation of light by the thin water layer above the cell (~2 mm) was negligible (< 0.05 % from 280–600 nm). Here $a_t(\lambda)$ (m^{-1}) is the sum of $a_{CDOM}(\lambda)$

and the absorption coefficient of pure water obtained from Pope and Fry (1997) and Buiteveld et al. (1994). S is the longitudinal cross section of the irradiation cell (0.0055 m^2) and L is the light pathlength of the cell, calculated as the squared root of the latitudinal cross section of the cell (0.0193 m), according to Osburn et al. (2001). Here $a_{CDOM}(\lambda)$ is the exponential-based average of two adjacent irradiation time points, since photobleaching approximately follows first-order kinetics (Del Vecchio and Blough, 2002; also see Section 3.1). AQYs of photomineralization (AQY_{DOC} in mol DOC (mol photons)$^{-1}$) and photomethanification (AQY_{CH4} in mol CH_4 (mol photons)$^{-1}$) were calculated as the rates of DOC loss and CH_4 production divided by the rate of photons absorbed by CDOM (i.e. $Q_{CDOM}(\lambda)$ in eq. 1) integrated over the wavelength ranges of interest. Broadband AQYs were computed over 280–600 nm for full-spectrum time-series irradiations and over UVB (280-320 nm), UVA (320-400 nm), and VIS (400-600 nm) for irradiations evaluating the spectral quality effect.

3. Results and Discussion

3.1. Photochemical O_2 consumption, bleaching and acidification

Figure 3 shows the time-course variations of [O_2], pH, the absorption coefficient at 330 nm ($a_{CDOM}(330)$), and the spectral slope ratio (S_R) defined as the ratio of the spectral slope coefficient between 275 nm and 295 nm to that between 350 nm and 400 nm. S_R has been used to characterize the source, molecular size, and photoprocessing of CDOM (Helms et al., 2008). Consistent with the results of previous studies (Gao and Zepp, 1998; Xie et al., 2004; Lou and Xie, 2006), irradiation led to photochemical O_2 consumption, absorbance bleaching, and acidification (i.e. decrease in pH). The temporal trends of these variables can be well

described by 3-parameter exponential decay equations (Table 1). At the end of irradiations, [O_2] decreased to 153.2 μmol L^{-1}, 890.6 μmol L^{-1}, and 42.2 μmol L^{-1} in the air-, O_2-, and N_2-treatments, respectively. The drop of [O_2] in the N_2-treatment occurred entirely within the first 48 h (Fig. 3A). These final O_2 concentrations indicate that oxic conditions were maintained in the air- and O_2-treatments throughout the irradiations while suboxic conditions persisted in the N_2-treatment. CDOM absorbance decreased throughout the UV and VIS regimes (Fig. 4), fastest in the O_2-treatment followed sequentially by the air- and N_2-treatment (Fig. 3B, Fig. 4), corroborating earlier findings (Gao and Zepp, 1998; Lou and Xie, 2006). The a_{CDOM} (330) declined by 75%, 56%, and 28% over the entire exposure period in the O_2-, air-, and N_2-treatment, respectively. S_R continuously increased over the entire irradiation period in the air- and O_2-treatments; S_R in the N_2-treatment increased with irradiation time up to ~120 h and became stable thereafter (Fig. 3C), suggesting a complete exhaustion of O_2. Notably, the changes in S_R for the three different O_2 levels nearly lined up together during the first 24-h irradiation but started diverging at ~48 h when [O_2] in the N_2-treatment dropped to a constant level (Fig. 3A). The pH in the air-treatment remained constantly below that in the O_2-treatment except near the end of irradiation where the two converged at a similar pH value of ~0.8 unit below the initial level (Fig. 3D). The ~0.5 unit drop of pH in the N_2-treatment took place largely within the initial 48 h, echoing the behavior of [O_2]. The tests utilizing different light filters indicate that photochemical O_2 consumption, bleaching and acidification decreased successively with the spectral composition of the incident light changing from UVB to UVA to VIS (Table 2), which conforms to the results of Lou and Xie (2006).

553 ### 3.2. Photomineralization

554 Note that photochemical DOC loss leads to production of CO_2 (in the form of
555 dissolved inorganic carbon, DIC) and carbon monoxide (CO), with DIC being the
556 main product (Miller and Zepp, 1995). As photomineralization rates reported in this
557 study were equated to DOC loss rates, the former also included the CO component.
558 Based on our unpublished AQY spectrum for CO photoproduction from CDOM in
559 Saguenay River surface water ($AQY_{CO}(\lambda) = 3.07 \times 10^{-10} \exp(5661/(149.1 + \lambda))$, where
560 λ is wavelength in nanometers), we estimated that the ratio of DIC to CO
561 photoproduction was 30.8. Photomineralization was thus overwhelmingly dominated
562 by DIC production in our study.

563 #### 3.2.1. Effect of $[O_2]$

564 [DOC] decreased exponentially with irradiation time as well (Fig. 5A and Table
565 1). The differences among the three O_2-treatments were rather small during the first
566 48 h and thereafter [DOC] in the N_2-treatment rapidly stabilized while [DOC] in the
567 air- and O_2-treatments continued to decline. Hence, $[O_2]$ in the N_2-treatment was a
568 limiting factor of photomineralization until $[O_2]$ decreased to a stable level (Fig. 5A).
569 Notably, the difference in the rate of [DOC] drawdown between the air- and
570 O_2-treatment was much smaller than that for $a_{CDOM}(330)$ (Fig. 3B), demonstrating that
571 photobleaching was far more sensitive to $[O_2]$ than photomineralization. While the
572 temporal trends of [DOC] were exponential, [DOC] decreased linearly with
573 absorbance photobleaching, with the slope becoming progressively steeper towards
574 deceasing initial $[O_2]$ (Fig. 5B). A closer examination of the data indicates that the
575 ratio of the fractional DOC loss to the fractional $a_{CDOM}(330)$ loss decreased from 0.82
576 in the N_2-treatment to 0.64 in the air-treatment to 0.54 in the O_2-treatment (Fig. 5C).

577 Similar results were obtained at the wavelengths of 254 nm, 300 nm, and 400 nm
578 (data not shown). Therefore, photochemical DOC loss proceeded more efficiently
579 under O_2-deficiency than under oxic conditions on a per-a_{CDOM}-loss basis, opposite to
580 the trend of the time-based DOC loss rate. In other words, higher fractions of CDOM
581 were mineralized under O_2-depletion than under oxygenation.

582

583 **3.2.2. Apparent quantum yields**

584 AQY_{DOC} decreased exponentially ($R^2 = 0.969$) in the N_2-treatment and remained
585 nearly constant ($1.50 \times 10^{-4} \pm 0.05 \times 10^{-4}$) in the air-treatment with respect to
586 photobleaching (Fig. 5D). In the O_2-treatment, AQY_{DOC} was invariable initially (up to
587 23% loss of $a_{CDOM}(330)$) and then increased linearly ($R^2 = 0.965$) with further
588 photobleaching. The decrease of AQY_{DOC} with photobleaching in the N_2-treatment
589 suggests that the removal of DIC precursors was faster than the bleaching of CDOM
590 under O_2 deficiency. Conversely, the results from the O_2- and air-treatments imply
591 that under oxic conditions the removal of DIC precursors was slower than or similar
592 to the bleaching of CDOM or that DIC precursors were regenerated during irradiation.
593 Although the mechanism of photoproduction of DIC is not well understood,
594 photodecarboxylation is considered to be involved (Miles and Brezonik, 1981).
595 However, Xie et al. (2004) found that neither the initial content nor the apparent loss
596 of carboxylic groups on DOM could account for the amount of DIC produced during
597 an extensive photobleaching of a Satilla River water sample. These authors thus
598 proposed that carboxylic groups are photochemically regenerated if
599 photodecarboxylation is the predominant pathway for DIC production. The trends of
600 AQY_{DOC} versus photobleaching observed under oxic conditions in the present study

601 are thus consistent with the supposition of Xie et al. (2004). Furthermore, the decrease
602 in pH (see section 3.1) indicates the formation of acidic photoproducts during
603 irradiation. Although the production of CO_2 (in the form of DIC) could have
604 contributed a large part to the pH decline, carboxylic acids are also known
605 photoproducts of CDOM (Moran and Zepp, 1997).

606 Data of AQY_{DOC} or AQY_{DIC} versus photobleaching (or absorbed doses) are
607 scarce. Previous studies on AQY_{DOC} or AQY_{DIC} often employed short-term
608 irradiations that led to minor losses of a_{CDOM} (e.g. Johannessen and Miller, 2001;
609 Reader and Miller, 2012). Results from the present study are pertinent to
610 medium-term exposures (up to 56% loss of $a_{CDOM}(330)$ in the air treatment). The
611 relatively invariable AQY_{DOC} across this photobleaching regime suggests that
612 AQY_{DOC} data obtained from short-term irradiations are applicable to modeling
613 photomineralization fluxes in the Saguenay River over medium-term exposures. Over
614 long-term exposures approaching a complete of loss of a_{CDOM}, Vähätalo and Wetzel
615 (2004) observed a decrease in AQY_{DOC} with photobleaching for water collected from
616 Lake Tuscaloosa in Alabama. It remains to be elucidated if the same is true for the
617 Saguenay River.

618 The irradiations employing light filters allowed us to evaluate the effect of light
619 quality on AQY_{DOC}. As shown in Table 2, AQY_{DOC} obtained from the air-treatment
620 decreased by ~12 times from UVB to UVA and further by 7 times from UVA to VIS.
621 The spectral dependence of AQY_{DOC} was lower for the N_2-treatment; AQY_{DOC} in
622 UVB was ~7 times that in UVA, which in turn was ~5 times that in VIS. The flatter
623 spectral dependence under the N_2- relative to air-treatment could be related to
624 different prevailing mechanisms for photomineralization, e.g. direct
625 photodecarboxylation under the N_2-treatment versus secondary photoprocesses

initiated by reactive oxygen species produced in the presence of molecular oxygen (Frimmel, 1994).

Full spectrum-based AQY_{DOC} obtained from the air-treatment in our study match closely those in Valkea-Kotinen lake (1.37×10^{-4}, derived from 300 nm to 700 nm, Vähätalo et al., 2000) and Pääjärvi lake (1.21×10^{-4}, derived from 190 nm to 800 nm, Aarnos et al., 2012) but an order lower than that in the Mackenzie river freshwater (1.0×10^{-3}–3.0×10^{-3}, derived from 280 nm to 500 nm, Osburn et al., 2009) and ~ 3 times higher than that in the Northern shelf in the Gulf of Mexico (5.6×10^{-6}, derived from 290 to 490 nm, Fichot and Benner, 2014). The difference may be attributed to the variation of photoreactivity of CDOM in different water bodies or different wavelength range for obtaining the AQY or both.

3.3.3. Implication for DOC cycling in the Saguenay River

Assuming negligible backscattering of light from the water column to the atmosphere, the depth-integrated photochemical DOC loss rate (P_{DOC}, mol C m^{-2} d^{-1}) in the euphotic zone of the Saguenay River can be calculated as:

$$P_{DOC} = Q \times \alpha_r \times R_a \times AQY_{DOC} \quad (2)$$

where Q (mol photons m^{-2} d^{-1}) is the global solar photon flux (280–600 nm) under clear-sky conditions at latitude 48.4 °N and is generated from the SMARTS2 model (Gueymard, 1995, 2001), α_r is the combination of two correction factors for reflection of light by cloud (0.8) and at the air-water interface (0.93) (Stubbins et al., 2006), and R_a is the fraction of light absorbed by CDOM in the photic zone, which is assumed to be 0.80 and vertically constant (Xie et al., 2012). AQY_{DOC} is the broadband (280–600

649 nm) photomineralization quantum yield determined during this study under the air
650 treatment ($1.50 \times 10^{-4} \pm 0.15 \times 10^{-4}$) and is assumed to be seasonally constant. P_{DOC}
651 was estimated to be $(2.97 \pm 0.30) \times 10^{-3}$ mol C m^{-2} d^{-1} in spring, $(3.67 \pm 0.37) \times 10^{-3}$
652 mol C m^{-2} d^{-1} in summer, $(1.71 \pm 0.17) \times 10^{-3}$ mol C m^{-2} d^{-1} in autumn, $(1.11 \pm 0.11) \times$
653 10^{-3} mol C m^{-2} d^{-1} in winter. These values yield an annual rate of 0.77 mol C m^{-2},
654 excluding ice-covered areas in spring (ice coverage: 0.11) and winter (ice coverage:
655 0.65) calculated from the 1971–2000 Canadian Ice Service database (CIS, 2001).
656 Combining the estimates of P_{DOC} with the area of the Saguenay River (300 km^2, 100
657 km long × 3 km wide) gives an annual rate of DOC photomineralization of 2.31×10^8
658 mol C. Based on the [DOC] near Chicoutimi (~583.3 μmol L^{-1}, this study and
659 Tremblay and Gagné, 2009) and a yearly averaged freshwater discharge of 1194 m^3
660 s^{-1} (Bélanger, 2003), the annual DOC input to the Saguenay River was calculated as
661 2.20×10^{10} mol C. DOC photomineralization thus accounts for 1% of the annual DOC
662 input. The majority of photomineralization of CDOM from the Saguenay River is
663 expected to take place after the CDOM is transported to the lower St. Lawrence
664 estuary and the Gulf of St. Lawrence, where it will be strongly diluted and thus
665 experience more efficient photooxidation.

666 The spectral dependence data of AQY_{DOC} (Table 2), combined with eq. 2,
667 allowed us to evaluate the relative contributions of UVB, UVA, and VIS to the
668 full-spectrum, depth-integrated photomineralization rate, arriving at 15, 41, and 44%,
669 respectively, for the air-treatment. Hence, VIS and UVA are the dominant
670 contributors while UVB is the least important.

671

672 **3.3. Photomethanification**

673 **3.3.1. Effect of [O_2]**

674 [CH_4] increased linearly with irradiation time (Fig. 6A), absorbance
675 photobleaching (Fig. 6B), and DOC loss (Fig. 6C) under the air- and O_2-treatments.
676 While the time-based rate of CH_4 photoproduction under the air-treatment (4.3 pmol
677 L^{-1} h^{-1}) was only 10% higher than under the O_2-treatment (3.9 pmol L^{-1} h^{-1}), the
678 $a_{CDOM}(330)$- and [DOC]-based rates differed by 57% (88 vs. 56 pmol L^{-1} m) and 30%
679 (5.7 vs. 4.4 pmol CH_4 (μmol DOC)$^{-1}$), respectively. [CH_4] in the N_2-treatment
680 increased sharply after an initial slow increment (Fig. 6A-C) that corresponded to a
681 major reduction of the residual [O_2] (Fig. 3A). The time-based production rate of CH_4
682 in the N_2-treatment decreased when approaching the end of irradiation (Fig. 6A),
683 whereas the $a_{CDOM}(330)$- and [DOC]-based rates continuously grew over the entire
684 exposure period (Fig. 6B, C). The time-course mean CH_4 production rate in the
685 N_2-treatment (32 pmol L^{-1} h^{-1}) was 7.4 times that in the air-treatment and 8.2 times
686 that in the O_2-treatment. The corresponding ratios increased to 56 and 88 on a
687 per-$a_{CDOM}(330)$ basis and 17 and 23 on a per-[DOC] basis.

688 Our results demonstrate that photomethanification is strongly favored under
689 O_2-deficiency but also occurs under oxygenated conditions. This observation
690 somewhat differs from that of Bange and Uher (2005) showing undetectable CH_4
691 photoproduction under oxic conditions but significant production under anoxia in the
692 presence of millimolar levels of acetone, a methyl (CH_3) radical precursor. Bange and
693 Uher (2005) proposed that photomethanification involves the formation of CH_3
694 radicals from CDOM-mediated photosensitized processes, followed by H-abstraction

by CH_3 radicals from a variety of potential substrates. These authors further reasoned that because of the reaction of dissolved O_2 with the CH_3 radical (Neta et al., 1996), the H-abstraction by CH_3 radicals, hence CH_4 production, is greatly suppressed by high dissolved O_2 concentrations. The different results between the two studies could thus have resulted from our sample containing more reactive CH_3 radical precursors, substrates for H-abstraction, and/or photosensitizing CDOM. It is also plausible that the CH_4 production rates reported by Bange and Uher (2005) are underestimates due to residual microbial activity in their filtered samples.

3.3.2. Apparent quantum yields

AQY_{CH4} in the air-treatment ($8.5 \times 10^{-10} \pm 0.4 \times 10^{-10}$) changed little with photobleaching but increased exponentially ($R^2 = 0.963$) in the N_2-treatment (range: $1.7–5.6 \times 10^{-9}$; mean: 3.5×10^{-9}) (Fig. 6D). AQY_{CH4} in the O_2-treatment varied between 3.2×10^{-10} and 8.6×10^{-10} (mean: $5.6 \times 10^{-10} \pm 2.2 \times 10^{-10}$) with the later irradiation stage giving relatively higher values than the earlier stage. On average, AQY_{CH4} was 4 times higher in the N_2-treatment than in the air-treatment, which in turn was 53% higher than in the O_2-treatment. At the end of irradiation, AQY_{CH4} in the N_2-treatment was 6.6 times that in the air-treatment. The rapid increases in CH_4 production (Fig. 6B) and AQY_{CH4} (Fig. 6D) with photobleaching in the N_2-treatment likely resulted from a continuing depletion of the residual O_2 in that sample. It should be noted that the stabilization of $[O_2]$ at 42.2 μmol L^{-1} towards the end of irradiation in the N_2-treatment (Section 3.1) could be ascribed to an ingress of O_2 from ambient air during sample transfer for $[O_2]$ determination, as alluded in Section 2.2. This artifact could have masked the decline of $[O_2]$.

719 Similar to the spectral dependence of AQY_{DOC}, AQY_{CH4} also decreased
720 sequentially from UVB to UVA to VIS for both the air- and N_2-treatments (Table 2).
721 However, AQY_{CH4} was strongly skewed towards UVB under the N_2 treatment.

722

723 **3.3.3. DMS as a precursor of CH_4**

724 An addition of 20 μmol L^{-1} DMS increased the rate of CH_4 photoproduction by
725 27–45% in the air-treatment (Fig. 7A) and by 14%–6400% in the N_2-treatment (Fig.
726 7B) over a time-series irradiation of up to 166.3 h. The difference between the
727 DMS-amended and the original sample increased with irradiation time. Irradiation of
728 samples containing varying DMS concentrations revealed an first-order kinetics of
729 CH_4 production with respect to [DMS] in the air-treatment but an Michaelis-Menten
730 type of kinetics in the N_2-treatment, with the production rate in the N_2-treatment two
731 orders of magnitude higher than in the air-treatment at [DMS] > 20 μmol L^{-1} (Fig. 8).

732 The similar patterns of the O_2 effect with and without the addition of DMS
733 suggest that CH_4 photoproduction from DMS may also proceed through the formation
734 of CH_3 radicals. DMS does not undergo direct photolysis, since it is transparent
735 within the spectrum of solar radiation reaching the earth's surface (McDiarmid, 1974).
736 However, DMS can be degraded by photosensitizing reactions, including those
737 initiated by CDOM (Brimblecombe and Shooter, 1986). The saturation of CH_4
738 production at elevated DMS concentrations in the N_2-treatment (Fig. 8) could be
739 interpreted as a limitation of the photosensitizing capacity of CDOM and/or the
740 availability of substrates for H-abstraction. Although the exact mechanism responsible
741 for DMS photodegradation in natural waters is not well established, the OH radical is
742 likely implicated (Bouillon and Miller, 2005; Williams et al., 2009). OH radicals in

743 natural waters are produced from CDOM photochemistry (Mopper and Zhou, 1990)
744 and photolysis of nitrate (Zafiriou and True, 1979) in the absence of O_2, with an
745 additional contribution from the (photo) Fenton reaction (Esplugas et al., 2002) in the
746 presence of O_2. As has been observed in gas-phase studies (Arsene et al., 2001), the
747 reaction of the OH radical with DMS may produce the CH_3 radical, though the
748 dominant product of this reaction is DMSO in the presence of O_2. The CH_3 radical
749 then abstracts a hydrogen atom from DMS itself (Arthur and Lee, 1976) or other
750 compounds such as thios (Neta et al., 1996) to produce CH_4. In brackish or saline
751 waters, the formation of CH_3 radicals may result from the reactions of DMS with the
752 Br_2^- and CO_3^- radicals which are preferentially produced via the reaction of the HO
753 radical with the bromide and carbonate/bicarbonate ions (True and Zafiriou, 1985).
754 The involvement of the CO_3^- in DMS oxidation has been confirmed by Bouillon and
755 Miller (2005), though the individual steps of this process are unclear.

756 Given that dissolved DMS concentrations in sunlit, oxic surface waters are
757 normally at nanomolar levels, it is unlikely that photodegradation of DMS can serve
758 as a significant source of CH_4 in the water column. However, cellular DMS
759 concentrations have been observed to reach up to 1.5–30 mmol (liter of cell volume)$^{-1}$
760 (Sunda et al., 2007), translating to a CH_4 production rate of 0.13–2.39 nmol (liter of
761 cell volume)$^{-1}$ h^{-1} under otherwise identical conditions. Photooxidation of cellular
762 DMS could thus provide a potentially significant source of CH_4 to waters that abound
763 with prolific DMS producers (e.g. *Phaeocystis*). In addition, cellular
764 dimethylsulfoniopropionate (DMSP) is often more abundant than cellular DMS
765 (Keller et al., 1989; Bucciarelli and Sunda, 2003) and therefore could also be a
766 potentially important precursor of photoproduced CH_4.

767

3.3.4. Implication for CH_4 cycling on regional and global scales

The depth-integrated photomethanification rate (P_{CH4}) in the Saguenay River can be estimated using eq. 2 by substituting AQY_{CH4} for AQY_{DOC}. Alternatively, it can be assessed by multiplying P_{DOC} by the slope of the fitted line for the air-treatment in Fig. 6C (i.e. 0.00057%). The former approach is adopted, arriving at $(1.69 \pm 0.08) \times 10^{-8}$ mol m^{-2} d^{-1} in spring, $(2.08 \pm 0.10) \times 10^{-8}$ mol m^{-2} d^{-1} in summer, $(9.70 \pm 0.48) \times 10^{-9}$ mol m^{-2} d^{-1} in fall, and $(6.33 \pm 0.31) \times 10^{-9}$ mol m^{-2} d^{-1} in winter. The annual total is calculated to be 4.36×10^{-6} mol m^{-2} with CH_4 photoproduction in ice-covered seasons ignored. It is not possible to compare the photoproduction rates with other CH_4 cycling terms in the Saguenay River such as microbial production and consumption rates and air-sea exchange fluxes, since the latter are unknown. The annual CH_4 photoproduction rate obtained for the Saguenay River is, however, about 12 % of the aerobic microbial CH_4 consumption rate in the surface Black Sea (Schmale et al., 2011) but is generally many orders of magnitude lower than sea-air fluxes in various estuarine and coastal environments, which frequently reach tens to hundreds of μmol m^{-2} d^{-1} (Bange et al., 1994).

As was the case for DOC (Section 3.3.3), the percent contributions of the three major wavelength ranges to the full-spectrum, depth-integrated CH_4 photoproduction were estimated using eq. 2 along with the spectral dependence data of AQY_{CH4} (Table 2). For the air-treatment, the contributions from UVA (39%) and VIS (35%) are similar while UVB only contributes 16%. As the attenuation of UVA and VIS is much slower than UVB in the water column, CH_4 photoproduction is expected to penetrate into relatively deep depths under oxic conditions. For the N_2-treatment, the percent contribution follows a descending order of UVA (43%) > UVB (40%) > VIS (17%), indicating that UVB is far more important than VIS under O_2-depleted

conditions.

Because the photomethanification efficiency of CDOM may change geographically, extrapolation of our results to other regions is speculative by nature. The current estimate of photodegradation of DOC in global open oceans ranges from 400–1700 Tg C yr^{-1} (Mopper et al., 2015), which exceeds the total riverine DOC input of ~260 Tg C yr^{-1} to global oceans (Raymond and Spencer, 2015). This DOC loss translates to a CH_4 photoproduction rate of (1.9–8.1) × 10^8 mol yr^{-1}, assuming that the ratio of CH_4 photoproduction to DOC loss (0.00057%) observed for the air-treatment in the present study is applicable to both riverine and marine DOC on global scales. These rates only account for 0.09–0.4% of the open-ocean CH_4 efflux of 2.3 × 10^{11} mol yr^{-1} (Bange et al., 1994) and 0.07–0.3% of the net CH_4 production of 2.3 μmol m^{-2} d^{-1} (2.6 × 10^{11} mol yr^{-1}) that is required to sustain the CH_4 supersaturation and outgassing loss in the upper 100 m of global open oceans (Reeburgh, 2007). However, our estimates of the CH_4 photoproduction rates are significant compared to microbial CH_4 oxidation rates in oxic open oceans that have been shown to be 0.15 nmol L^{-1} yr^{-1} in waters of <10 years old (equivalent to 5.4 × 10^9 mol yr^{-1} if scaled to the upper 100 m layer) and 10^{-4} nmol L^{-1} yr^{-1} in aged waters (equivalent to 1.3 × 10^8 mol yr^{-1} if scaled to waters deeper than 100 m) (Reeburgh, 2007). Notably, our estimates do not take into account CH_4 that could be produced photochemically from anoxic and low-oxygen microenvironments present in decaying organic particles such as planktonic detritus and fecal pellets (Alldredge and Cohen, 1987). Since AQY_{CH4} under anoxic conditions is up to 7 times that at air-saturation (Section 3.3.2) and since organic particles are likely more photoreactive than CDOM (Zafiriou, 2002), particularly at VIS wavelengths (Song et al., 2013), it is plausible that the particle-based CH_4 photoproduction could be more important that the CDOM

818 counterpart.

819 The present study demonstrates that CH_4 photoproduction is favored by UVB
820 under O_2-deficiency. Given that the surface ocean in the Archean was anoxic before
821 O_2 accumulation in the atmosphere 2.32 billion years ago (Bekker et al., 2004) and
822 that UVB in the Archean was ~3 times the present-day level (Cockell, 1998), the CH_4
823 photoproduction rate in the Archean ocean can be approximately inferred from our
824 results for the N_2 treatment by summing 3 times the production under UVB, 1 time
825 the production under UVA, and 1 time the production under VIS, giving 9.78×10^{-8}
826 mol CH_4 m^{-2} d^{-1}. This value corresponds to only 0.7% of the CH_4 flux density in the
827 Archean (1.47×10^{-5} mol m^{-2} d^{-1}) that was required to maintain a CH_4 mixing ratio of
828 100 ppm in the Archean atmosphere (Bange and Uher, 2005). Note that this estimate
829 is based on the assumption that AQY_{CH4} and the fraction of solar radiation absorbed
830 by CDOM in the Archean ocean were similar to those adopted in this study. It should
831 also be pointed out that N_2-purging must have depleted the volatile precursors of the
832 methyl radical in our samples and that the Archean ocean likely contained higher
833 concentrations of CH_4 precursors such as acetone (Bange and Uher, 2005) than does
834 the present ocean, thereby leading to an underestimate of CH_4 photoproduction in the
835 Archean ocean.

836

837 **Summary and Future Work**

838 Rates of photomineralization and photomethanification of CDOM from the
839 Saguenay River were determined at three widely different [O_2]s (suboxic,
840 air-saturated, and oxygenated) over medium-term exposure to simulated solar
841 radiation. Photomineralization increased linearly with absorbance photobleaching.

While the photochemical DOC loss rate increased with increasing [O_2], the ratio of the fractional DOC loss to the fractional a_{CDOM} loss trended oppositely. Photochemical breakdown of CDOM led to a higher degree of mineralization (i.e. DIC production) under suboxic conditions than under oxic conditions. AQY_{DOC} increased, decreased, and remained fairly constant with photobleaching under oxygenated, suboxic, and air-saturated conditions, respectively. AQY_{DOC} (or AQY_{DIC}) determined under air-saturation with short-term irradiations can be applied to medium-term exposures for the Saguenay River. The spectral dependence of AQY_{DOC} revealed by this study, in conjunction with the solar irradiance spectrum, points to VIS and UVA being the primary drivers for photomineralization in the water column of the Saguenay River. The photomineralization rate in the Saguenay River was estimated to be 2.31×10^8 mol C yr^{-1}, accounting for only 1% of the annual DOC input into this system.

Photomethanification occurred under both suboxic and oxic conditions and increased with decreasing [O_2], with the rate under suboxic conditions ~7–8 times that under oxic conditions. Photoproduction of CH_4 under oxic conditions increased linearly with photochemical losses of DOC and absorbance, rendering photomineralization and photobleaching to be proxies for photomethanification. Under air-saturation, 0.00057% of photochemical DOC loss in the Saguenay River surface water went to CH_4, giving a photochemical CH_4 production rate of 4.36×10^{-6} mol m^{-2} yr^{-1} in the Saguenay River and, by extrapolation, of $(1.9–8.1) \times 10^8$ mol yr^{-1} in the global ocean. AQY_{CH4} changed little with photobleaching under air-saturation but increased exponentially under suboxic conditions. On a depth-integrated basis, VIS prevailed over UVB in controlling CH_4 photoproduction under air-saturation while the opposite held true under O_2-deficiency. Spiking with dissolved DMS

867 increased CH_4 photoproduction, particularly under O_2-deficiency; DMS at nanomolar
868 ambient concentrations in surface oceans is, however, unlikely a significant CH_4
869 precursor. Although CDOM-based CH_4 photoproduction is estimated to be only a
870 marginal contributor to both the modern and Archean atmospheric CH_4 budgets, its
871 magnitude can be comparable to those of microbial CH_4 oxidation in modern oxic
872 oceans.

873 Future work should extend sampling coverage, quantify CH_4 photoproduction
874 from particulate organic matter, and elucidate the mechanisms of
875 photomethanification of organic matter in natural waters, including tests on other
876 precursors of CH_3 radicals such as DMSP, dimethyl sulfoxide (DMSO), acetonitrile,
877 methionine, methylamine and methyl ester that are naturally present in aquatic
878 environments. For river and riverine-impacted coastal waters, particular attention
879 should be paid to methoxy-substituted phenols in dissolved lignin, since these
880 compounds are highly susceptible to photodegradation (Benner and Kaiser, 2011) and
881 since the methoxy groups in certain lignin model phenols have been demonstrated to
882 be efficient precursors of CH_4 under anaerobic conditions (Weir et al., 1995). Anoxic
883 microniches in particulate organic matter and phytoplankton cells containing elevated
884 concentrations of methylated compounds, such as DMS, DMSP, and DMSO, may
885 provide potential hotspots for CH_4 photoproduction.

886 **Acknowledgements**

887 This work was supported by HX's NSERC Discovery Grant and by the National
888 Natural Science Foundation of China (NSFC) (Grant# 41006040). YZ was supported
889 by a postdoctoral fellowship awarded by the Shandong International Exchange
890 Association. Claude Belzile measured bacterial populations and DOC concentrations.

891

892 **References**

893 Aarnos, H., Ylöstalo, P., and Vähätalo, A. V.: Seasonal phototransformation of
894 dissolved organic matter to ammonium, dissolved inorganic carbon, and labile
895 substrates supporting bacterial biomass across the Baltic Sea, J. Geophys. Res.,
896 117, G01004, doi: 10.1029/2010JG001633, 2012.

897 Alldredge, A. L. and Cohen, Y.: Can microscale chemical patches persist in the sea -
898 microelectrode study of marine snow, fecal pellets, Science, 235, 689–691, 1987.

899 Anesio, A. M. and Granéli, W.: Increased photoreactiviey of DOC by acidification:
900 Implications for the carbon cycle in humic lakes, Limnol. Oceanogr., 48(2), 735–
901 744, 2003.

902 Arsene, C., Barnes, I., Becker, K. H., and Mocanu, R.: FT-IR product study on the
903 photo-oxidation of dimethyl sulphide in the presence of NOx—temperature
904 dependence, Atmos. Environ., 35, 3769–3780,
905 doi:10.1016/S1352-2310(01)00168-6, 2001.

906 Arthur, N. L. and Lee, M. S.: Reactions of methyl radicals. 1. Hydrogen abstraction
907 from dimethyl sulfide, Aust. J. Chem., 29, 1483–1492, 1976.

908 Babin, M., Stramski, D., Ferrari, G. M., Claustre, H., Bricaud, A., Obolensky, G., and
909 Hoepffner, N.: Variations in the light absorption coefficients of phytoplankton,
910 nonalgal particles, and dissolved organic matter in coastal waters around Europe,
911 J. Geophy. Res., 108, 3211, doi:10.1029/2001JC000882, 2003.

912 Bange, H. W., Bartell, U. H., Rapsomanikis, S., and Andreae, M. O.: Methane in the
913 Baltic and North Seas and a reassessment of the marine emissions of methane,
914 Global Biogeochem. Cy., 8, 465–480, 1994.

915 Bange, H. W. and Uher, G.: Photochemical production of methane in natural waters:
916 implications for its present and past oceanic source, Chemosphere, 58, 177–183,
917 2005.

918 Bekker, A., Holland, H. D., Wang, P. L., Rumble, D., Stein, H. J., Hanna, J. L.,
919 Coetzee, L. L., and Beukes, N. J.: Dating the rise of atmospheric oxygen, Nature,
920 427, 117–120, 2004.

921 Bélanger, C.: Observation and modelling of a renewal event in the Sagueany Fjord,
922 Ph.D. thesis, Université du Québec à Rimouski, Rimouski, Québec, 2003.

923 Benner, R. and Kaiser, K.: Biological and photochemical transformations of amino
924 acids and lignin phenols in riverine dissolved organic matter, Biogeochemistry,
925 102, 209–222, doi:10.1007/s10533-010-9435-4, 2011.

926 Bertilsson, S. and Tranvik, L. J.: Photochemical transformation of dissolved organic
927 matter in lakes, Limnol. Oceanogr., 45, 753–762, doi: 10.4319/lo.2000.45.4.0753,
928 2000.

929 Bouillon, R. C. and Miller, W. L.: Photodegradation of dimethyl sulfide (DMS) in
930 natural waters: Laboratory assessment of the nitrate-photolysis-induced DMS
931 oxidation, Environ. Sci. Technol., 39, 9471–9477, doi:10.1021/es048022z, 2005.

932 Bourgault, D., Galbraith, P. S., and Winkler, G.: Exploratory observations of winter
933 oceanographic conditions in the Saguenay Fjord, Atmosphere-Ocean, 50:1, 17–
934 30, doi: 10.1080/07055900.2012.659844, 2012.

935 Brimblecombe, P. and Shooter, D.: Photo-oxidation of dimethylsulphide in aqueous
936 solution, Mar. Chem., 19, 343–353, 1986.

937 Bucciarelli, E. and Sunda, W. G.: Influence of CO_2, nitrate, phosphate, and silicate
938 limitation on intracellular dimethylsulfoniopropionate in batch cultures of the
939 coastal diatom Thalassiosira Pseudonana, Limnol. Oceanogr., 48, 2256–2265,
940 2003.

941 Buiteveld, H., Hakvoort, J. M. H., and Donze, M.: The optical properties of pure
942 water. In: SPIE Proceedings on Ocean Optics XII, edited by J. S. Jaffe, 2258,
943 174−183, 1994.

944 Cicerone, R. J. and Oremland, R. S.: Biogeochemical aspects of atmospheric methane,
945 Global Biogeochem. Cy., 2(4), 299–327, doi:10.1029/GB002i004p00299, 1988.

946 CIS (Canadian Ice Service): Sea Ice Climatic Atlas: East Coast of Canada, 1971–2000,
947 Canadian Government Publishing, Ottawa, 2001.

948 Cockell, C. S.: Biological effects of high ultraviolet radiation on early Earth—A
949 theoretical evaluation, J. Theor. Biol., 193, 717–729, 1998.

950 Cory, R. M., Ward, C. P., Crump, B. C., and King, G. W.: Sunlight controls water
951 column processing of carbon in arctic fresh waters, Science, 345,

952 doi:10.1126/science.1253119, 2014.

953 Damm, E., Kiene, R. P., Schwarz, J., Falck, E., and Dieckmann, G.: Methane cycling
954 in Arctic shelf water and its relationship with phytoplankton biomass and DMSP,
955 Mar. Chem., 109, 45–59, doi:10.1016/j.marchem.2007.12.003, 2008.

956 Damm, E., Helmke, E., Thoms, S., Schauer, U., Nöthig, E., Bakker, K., and Kiene, R.
957 P.: Methane production in aerobic oligotrophic surface water in the central Arctic
958 Ocean, Biogeosciences, 7, 1099–1108, doi:10.5194/bg-7-1099-2010, 2010.

959 Damm, E., Thoms, S., Beszczynska-Möller, A., Nöthig, E. M., and Kattner, G.:
960 Methane excess production in oxygen-rich polar water and a model of cellular
961 conditions for this paradox, Polar Science, in press, doi:
962 10.1016/j.polar.2015.05.001, 2015.

963 Del, Vecchio, R. and Blough, N. V.: Photobleaching of chromophoric dissolved
964 organic matter in natural waters: Kinetics and modelling, Mar. Chem., 78, 231–
965 253, 2002.

966 Drainville, G.: Le fjord du Saguenay: I. Contribution à l'océanographie, Naturaliste
967 Can. 95 (4), 809–855, 1968.

968 Esplugas, S., Giménez, J., Contreras, S., Pascual, E., and Rodríguez, M.: Comparison
969 of different advanced oxidation processes for phenol degradation, Water Res., 36,
970 1034–1042, 2002.

971 Fichot, C. G. and Benner, R.: The fate of terrigenous dissolved organic carbon in a

river-influenced ocean margin, Global Biogeochem. Cy., 28, 1–19, doi: 10.1002/2013GB004670, 2014.

Florez-Leivaa, L., Dammb, E., and Farías, L.: Methane production induced by dimethylsulfide in surface water of an upwelling ecosystem, Prog. Oceanogr., 112–113, 38–48, doi:10.1016/j.pocean.2013.03.005, 2013.

Frimmel, F. H.: Photochemical aspects related to humic substances, Environ. Int., 20 (3), 373–385, 1994.

Gao, H. and Zepp, R. G.: Factors influencing photoreactions of dissolved organic matter in a coastal river of the southeastern United States, Environ. Sci. Technol., 32, 2940–2946, 1998.

Gueymard, C.: SMARTS2, a simple model of the atmospheric radiative transfer of sunshine: algorithms and performance assessment, Professional Paper FSEC-PF-270-95, Florida Solar Energy Center, 1995.

Gueymard, C.: Parameterized transmittance model for direct beam and circumsolar spectral irradiance, Sol. Energy, 71, 325–346, 2001.

Helms, J. R., Stubbins, A., Ritchie, J. D., Minor E. C., Kieber, D. J., and Mopper, K.: Absorption spectral slopes and slope ratios as indicators of molecular weight, source, and photobleaching of chormophoric dissolved organic matter, Limnol. Oceanogr., 53 (3), 955–969, 2008.

Hong, J., Xie, H., Guo, L. D., and Song, G. S.: Carbon monoxide photoproduction:

992 implications for photoreactivity of Arctic permafrost-derived soil dissolved
993 organic matter, Environ. Sci. Technol, 48, 9113–9121, 2014.

994 Hu, C., Muller-Karger, F. E., and Zepp, R. G.: Absorbance, absorption coefficient,
995 and apparent quantum yield: A comment on common ambiguity in the use of
996 these optical concepts, Limnol. Oceanogr., 47, 1261–1267. 2002.

997 IPCC: "Climate change 2013: the physical science basis," in Contribution of Working
998 Group I to the Fifth Assessment Report of the Intergovernmental Panel on
999 Climate Change, Cambridge, UK: Cambridge University Press, 2013.

1000 Johannessen, S. C. and Miller, W. L.: Quantum yield for the photochemical
1001 production of dissolved inorganic carbon in seawater, Mar. Chem., 2001, 76,
1002 271–283.

1003 Karl, D. M., Beversdorf, L., Bjorkman, K. M., Church, M. J., Martinez, A., and
1004 DeLong, E. F.: Aerobic production of methane in the sea, Nat. Geosci., 1, 473–
1005 478, 2008.

1006 Keller, M. D., Bellows, W. K., and Guillard, R. R. L.: Dimethylsulfide production in
1007 marine phytoplankton, In: Saltzman E. S. and Cooper W. J. (eds.), Biogenic
1008 Sulfur in the Environment, American Chemical Society, pp. 167–182, 1989.

1009 Kieber, D. J., McDaniel, J., and Mopper, K.: Photochemical source of biological
1010 substrates in sea water: implications for carbon cycling, Nature, 341, 637–639,
1011 doi: 10.1038/341637a0, 1989.

1012 Liss, P. S., Marandino, C. A., Dahl, E. E., Helmig, D., Hintsa, E. J., Hughes, C.,
1013 Johnson, M. T., Moore, R. M., Plane, J. M. C., Quack, B., Singh, H. B., Stefels,
1014 J., von Glasow, R., and Williams, J.: Short-lived trace gases in the surface ocean
1015 and the atmosphere, p 1–54. In Liss, P. S. and Johnson, M. T. (eds),
1016 Ocean-atmosphere interactions of gases and particles, Springer Open, 2014.

1017 Lou, T. and Xie, H.: Photochemical alteration of molecular weight of dissolved
1018 organic matter, Chemosphere, 65, 2333–2342, 2006.

1019 McDiarmid, R.: Assignment of rydberg and valence transitions in the electronic
1020 spectrum of dimethylsulphide, J. Chem. Phys., 61, 274–281, 1974.

1021 Metcalf, W. W., Griffin, B. M., Cicchillo, R. M., Gao, J., Janga, S. C., Cooke, H. A.,
1022 Circello, B. T., Evans, B. S., Martens-Habbena, W., Stahl, D. A., and van der
1023 Donk, W. A.: Synthesis of methylphosphonic acid by marine microbes: a source
1024 for methane in the aerobic ocean, Science, 337, 11104–11107, 2012.

1025 Miles, C. J. and Brezonik, P. L.: Oxygen consumption in humic-colored waters by a
1026 photochemical ferrous-ferric catalytic cycle, Environ. Sci. Technol., 15 (9),
1027 1089–1095, doi: 10.1021/es00091a010, 1981.

1028 Miller, W. L. and Zepp, R. G.: Photochemical production of dissolved inorganic
1029 carbon from terrestrial organic matter: significance to the oceanic organic carbon
1030 cycle, Geophys. Res. Lett., 22, 417–420, 1995.

1031 Miller, W. L., Moran, M. A., Sheldon, W. M., Zepp, R. G., and Opsahl, S.:
1032 Determination of apparent quantum yield spectra for the formation of

biologically labile photoproducts, Limnol. Oceanogr., 47, 343–352, 2002.

Molot, L. A., Hudson, J. J., Dillon, P. J., and Miller, S. A.: Effect of pH on photo-oxidation of dissolved organic carbon by hydroxyl radicals in a coloured softwater stream, Aquat. Sci., 67 (2), 189–195, 2005.

Mopper, K. and Kieber, D. J.: Photochemistry and the cycling of carbon, sulfur, nitrogen and phosphorus, In Hansell, D. A. and Carlson, C. A. (eds.), Biogeochemistry of marine dissolved organic matter, Academic Press, San Diego, USA, 456–508, 2002.

Mopper, K., Kieber, D. J., and Stubbins, A.: Marine Photochemistry of Organic Matter: Processes and Impacts. In Hansell, D. A. and Carlson, C. A. (Eds), Biogeochemistry of marine dissolved organic matter (second edition), Academic Press, San Diego, USA, 389–450, 2015.

Mopper, K. and Zhou, X. L.: Hydroxyl radical photoproduction in the sea and its potential impact on marine processes, Science, 250, 661–664, 10.1126/science.250.4981.661, 1990.

Moran, M. A. and Zepp, R. G.: Role of photoreactions in the formation of biologically labile compounds from dissolved organic matter, Limnol. Oceanogr., 42(6), 1307–1316, 1997.

Neta, P., Grodkowski, J., and Ross A. B.: Rate constants for reactions of aliphatic carbon–centered radicals in aqueous solution, J. Phys. Chem. Ref. Data, 25, 709, http://dx.doi.org/10.1063/1.555978, 1996.

1054 Obernosterer, I. and Benner, R.: Competition between biological and photochemical
1055 processes in the mineralization of dissolved organic carbon, Limnol. Oceanogr.,
1056 49, 117–124, doi: 10.4319/lo.2004.49.1.0117, 2004.

1057 Osburn, C. L., Retamal, L., and Vincent, W. F.: Photoreactivity of chromophoric
1058 dissolved organic matter transported by the Mackenzie River to the Beaufort Sea,
1059 Mar. Chem., 115, 10–20, doi:10.1016/j.marchem.2009.05.003, 2009.

1060 Osburn, C. L., Zagarese, H. E., Morris, D. P., Morris, Hargreaves, B. R., and Cravero,
1061 W. E.: Calculation of spectral weighting functions for the solar photobleaching
1062 of chromophoric dissolved organic matter in temperate lakes, Limnol. Oceanogr.,
1063 46, 1455–1467, 2001.

1064 Pope, R. M. and Fry, E. S.: Absorption spectrum (380–700nm) of pure water, II,
1065 Integrating cavity measurements, Appl. Opt., 36, 8710–8723, 1997.

1066 Raymond, P. A. and Spencer, R. G. M.: Riverine DOM, In Hansell, D. A. and Carlson,
1067 C. A. (Eds), Biogeochemistry of marine dissolved organic matter (second
1068 edition), Academic Press, San Diego, USA, 509–533, 2015.

1069 Reader, H. E. and Miller, W. L.: Variability of carbon monoxide and carbon dioxide
1070 apparent quantum yield spectra in three coastal estuaries of the South Atlantic
1071 Bight, Biogeosciences, 9, 4279–4294, doi:10.5194/bg-9-4279-2012, 2012.

1072 Reeburgh, W. S.: Oceanic methane biogeochemistry, Chem. Rev., 107, 486–513,
1073 2007.

1074 Roy, R., Campbell, P. G. C., Prémont, S., and Labrie, J.: Geochemistry and toxicity of
1075 aluminum in the Saguenay River, Québec, Canda, in relation to discharges from
1076 an alumiunum smelter, Environ. Toxicol. Chem., 19, 2457–2466, 2000.

1077 Schafer, C. T., Smith, J. N., and Côté, R.: The Saguenay Fjord: A major tributary to
1078 the St. Lawrence Estuary. In El-Sabh M. I. and Silverberg N. (Eds.),
1079 Oceanography of a large-scale estuarine system, the St. Lawrence, Vol 39,
1080 Springer-Verlag, New York, USA, 378–420, 1990.

1081 Schmale, O., Haeckel, M., and McGinnis, D. F.: Response of the Black Sea methane
1082 budget to massive short-term submarine inputs of methane, Biogeosciences, 8,
1083 911–918, 2011.

1084 Song, G., Xie, H., Belanger, S., Leymarie, E., and Babin, M.: Spectrally resolved
1085 efficiencies of carbon monoxide (CO) photoproduction in the western Canadian
1086 Arctic: particles versus solutes, Biogeosciences, 10, 3731–3748, 2013.

1087 Stubbins, A., Uher, G., Law, C. S., Mopper, K., Robinson, C., and Upstill-Goddard, R.
1088 C.: Open-ocean carbon monoxide photoproduction, Deep-Sea Res. II, 53, 1695–
1089 1705, 2006.

1090 Sunda, W. G., Hardison, R., Kiene, R. P., Bucciarelli, E., and Harada, H.: The effect
1091 of nitrogen limitation on cellular DMSP and DMS release in marine
1092 phytoplankton: climate feedback implications, Aquat. Sci., 69, 341–351, 2007.

1093 Tilbrook, B. D. and Karl, D. M.: Methane sources, distributions, and sinks from
1094 California coastal waters to the oligotrophic North Pacific gyre, Mar. Chem., 49,

51–64, 1995.

Tremblay, L. and Gagné, J. P.: Organic matter distribution and reactivity in the waters of a large estuarine system, Mar. Chem., 116, 1–12, 2009.

True, M. B. and Zafiriou, O. C.: Reaction of OH radical with seawater - formation of Br_2^- and subsequent reaction with carbonate, Abstracts of papers of the American Chemical Society, 189, 3, 1985.

Vähätalo, A.V. and Wetzel, R. G.: Photochemical and microbial decomposition of chromophoric dissolved organic matter during long (months–years) exposures, Mar. Chem., 89, 313–326, doi:10.1016/j.marchem.2004.03.010, 2004.

Vähätalo, A.V., Salkinoja-Salonen, M., Taalas, P., and Salonen, K.: Spectrum of the quantum yield for photochemical mineralization of dissolved organic carbon in a humic lake, Limnol. Oceanogr., 45, 664–676, 2000.

Weller, D. I., Law, C. S., Marriner, A., Nodder, S. D., Chang, F. H., Stephens, J. A., Wilhelm, S. W., Boyd, P. W., and Sutton, P. J. H.: Temporal variation of dissolved methane in a subtropical mesoscale eddy during a phytoplankton bloom in the southwest Pacific Ocean, Prog. Oceanogr., 116: 193–206, 2013.

Weir, N. A., Arct, J., and Ceccarellik, A.: Photodegradation of lignin model compounds: part 2—substituted stilbenes, Polymer Degradation and Stability, 47, 289–297, 1995.

Williams, M. B., Campuzano-Jost, P., Hynes, A. J., and Pounds A. J.: Experimental

1115 and theoretical studies of the reaction of the OH radical with alkyl sulfides: 3.
1116 kinetics and mechanism of the OH initiated oxidation of dimethyl, dipropyl, and
1117 dibutyl sulfides: Reactivity trends in the alkyl sulfides and development of a
1118 predictive expression for the reaction of OH with DMS, J. Phys. Chem., A 113,
1119 6697–6709, 2009.

1120 Xie, H., Andrews, S. S., Martin, W. R., Miller, J., Ziolkowski, L., Taylor, C. D., and
1121 Zafiriou, O. C.: Validated methods for sampling and headspace analysis of
1122 carbon monoxide in seawater, Mar. Chem., 77, 93–108, 2002.

1123 Xie, H., Zafiriou, O. C., Cai, W. J., Zepp, R. G., and Wang, Y.: Photooxidation and its
1124 effects on the carboxyl content of dissolved organic matter in two coastal rivers
1125 in the southeastern United States, Environ. Sci. Technol., 38, 4113–4119, 2004.

1126 Xie, H., Zhang, Y., Lemarchand, K., and Poulin, P.: Microbial carbon monoxide
1127 uptake in the St. Lawrence estuarine system, Mar. Ecol. Prog. Ser., 389, 17–29,
1128 doi: 10.3354/meps08175, 2009.

1129 Xie, H., Aubry, C., Bélanger, S., and Song, G.: The dynamics of absorption
1130 coefficients of CDOM and particles in the St. Lawrence estuarine system:
1131 Biogeochemical and physical implications, Mar. Chem., 128–129, 44–56, 2012.

1132 Zafiriou, O. C.: Sunburnt organic matter: Biogeochemistry of light-altered substrates,
1133 Limnol. Oceanogr. Bull., 11, 69–86, doi: 10.1002/lob.200211469, 2002.

1134 Zafiriou, O. C. and True, M. B.: Nitrate photolysis in seawater by sunlight, Mar.
1135 Chem., 8, 33–42, doi:10.1016/0304-4203(79)90030-6, 1979.

1136 Zindler, C., Bracher, A., Marandino, C. A., Taylor, B., Torrecilla, E., Kock, A., and

1137 Bange, H. W.: Sulphur compounds, methane, and phytoplankton: interactions
1138 along a north–south transit in the western Pacific Ocean, Biogeosciences, 10,
1139 3297–165, 2013.

Table 1. Fitted parameters for function y = a + b*exp (-c*x), where x is irradiation time in hours. F_O_2 stands for fraction of dissolved [O_2]. [DOC] and [O_2] are in mmol L^{-1}, and $a_{CDOM}(330)$ is in m^{-1}.

y	O_2-treatment				Air-treatment				N_2-treatment			
	a	b	c	R^2	a	b	c	R^2	a	b	c	R^2
DOC	315.4	269.8	0.0051	0.987	427.5	155.7	0.0108	0.997	506.9	72.9	0.0277	0.992
$a_{CDOM}(330)$	2.69	21.63	0.011	0.994	9.83	14.63	0.0174	0.999	17.4	6.95	0.0252	0.998
pH	6.17	1.10	0.0097	0.963	6.39	0.828	0.0237	0.996	6.67	0.542	0.060	0.908
F_O_2	0.834	0.170	0.0095	0.935	0.528	0.463	0.0136	0.992	0.800	0.200	0.0596	0.980
Initial [O_2]	1023.0				271.2				53.1			

Table 2. AQYs of DOC and CH_4 and rates of $a_{CDOM}(330)$ loss, O_2 consumption and pH decrease under three light regimes (UVB, UVA, and VIS) in air- and N_2-treatments. Values are in mean ± SD.

		AQY_{DOC} ($\times10^{-4}$)	AQY_{CH4} ($\times10^{-9}$)	$a_{CDOM}(330)$ loss (m^{-1} h^{-1})	O_2 loss (μmol L^{-1} h^{-1})	pH decrease ($\times10^{-3}$ h^{-1})
Air	UVB	72.1±4.74	38.9±2.01	0.13±0.005	1.67±0.11	2.76±0.35
	UVA	6.24±0.36	3.55±0.24	0.06±0.004	0.45±0.10	1.61±0.23
	VIS	0.93±0.06	0.42±0.02	0.03±0.003	0.02±0.01	0.69±0.08
N_2	UVB	28.2±1.50	372.7±8.9	0.14±0.005	1.12±0.04	1.47±0.82
	UVA	4.19±0.90	12.76±1.24	0.09±0.002	0.25±0.05	1.23±0.18
	VIS	0.77±0.03	0.67±0.05	0.05±0.004	0.15±0.03	0.51±0.27

Figure Captions

Fig. 1. Map of the Saguenay River. Water samples were taken at the riverside of Chicoutimi.

Fig. 2. UV and VIS spectra of the solar-simulated radiation and noontime clear-sky solar radiation recorded at Rimouski (48.453° N, 68.511° W), Québec, on 24 May 2014.

Fig. 3. Fraction of dissolved O_2 (A), $a_{CDOM}(330)$ (B), S_R (C), and pH (D) versus irradiation time.

Fig. 4. Comparison of absorption spectra before and after full-spectrum irradiations.

Fig. 5. [DOC] versus irradiation time (A) and $a_{CDOM}(330)$ (B), fractional loss of DOC versus fractional loss of $a_{CDOM}(330)$ (C), and AQY_{DOC} versus fraction of initial $a_{CDOM}(330)$ (D). Lines in panels A and B are best fits of the data. Fitted equations for panel A are presented in Table 1.

Fig. 6. [CH_4] versus irradiation time (A), $a_{CDOM}(330)$ (B) and [DOC] (C), and AQY_{CH4} versus fraction of initial $a_{CDOM}(330)$ (D). Lines in panels A, B and C are best fits of the data.

Fig. 7. Effect of DMS spiking (20 μmol L^{-1}) on CH_4 photoproduction in a time-series irradiation under air- and N_2-treatments (A & B).

Fig. 8. Photoproduction rate of CH_4 as a function of added [DMS].

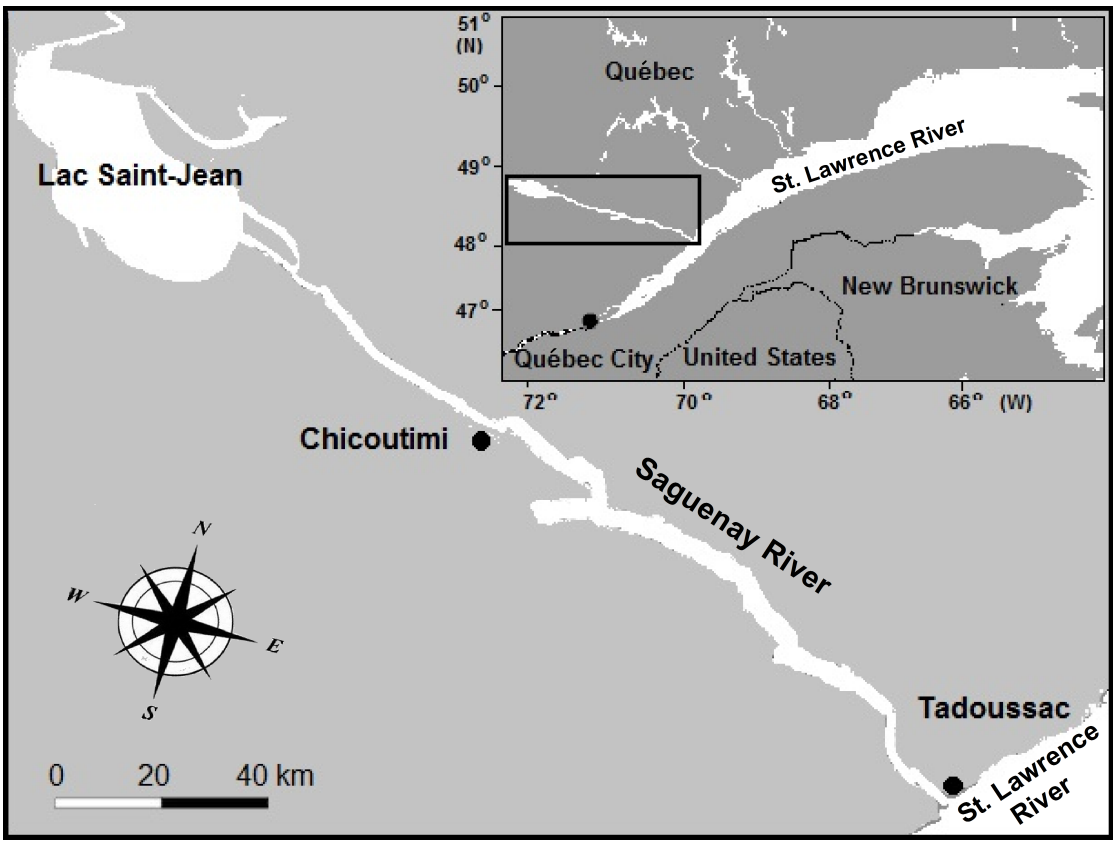

Fig. 1. Map of the Saguenay River. Water samples were taken at the riverside of Chicoutimi.

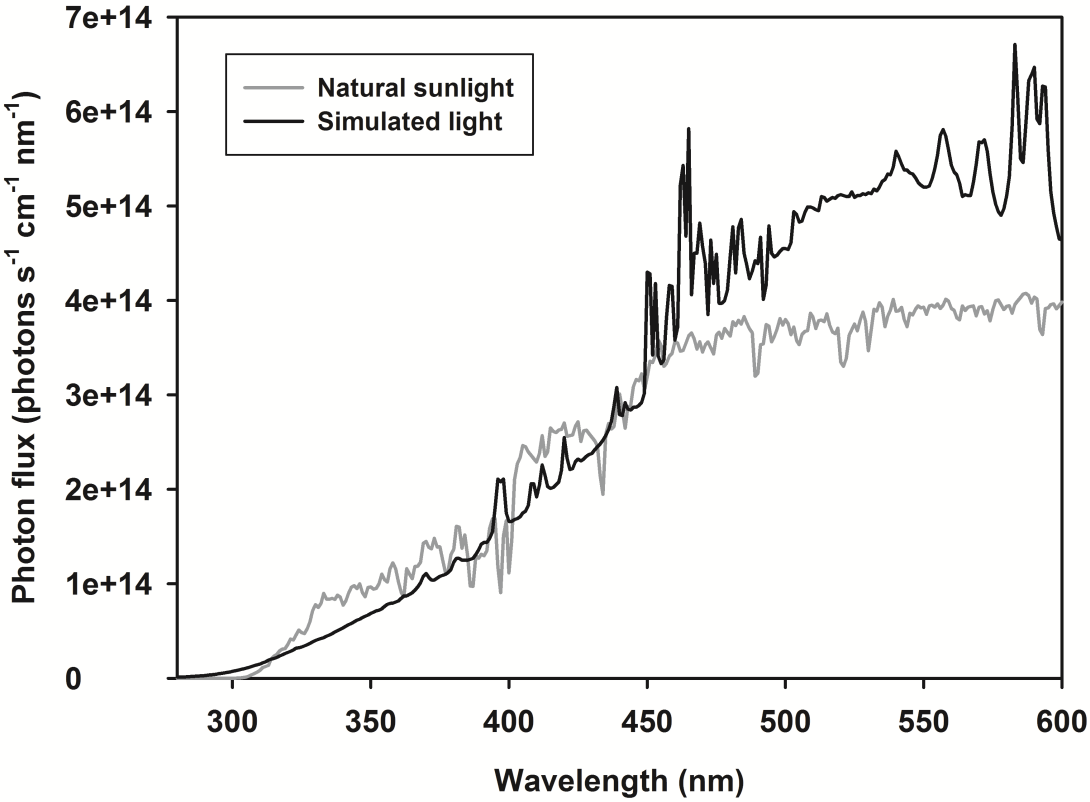

Fig. 2. UV and VIS spectra of the solar-simulated radiation and noontime clear-sky solar radiation recorded at Rimouski (48.453° N, 68.511° W), Québec, on 24 May 2014.

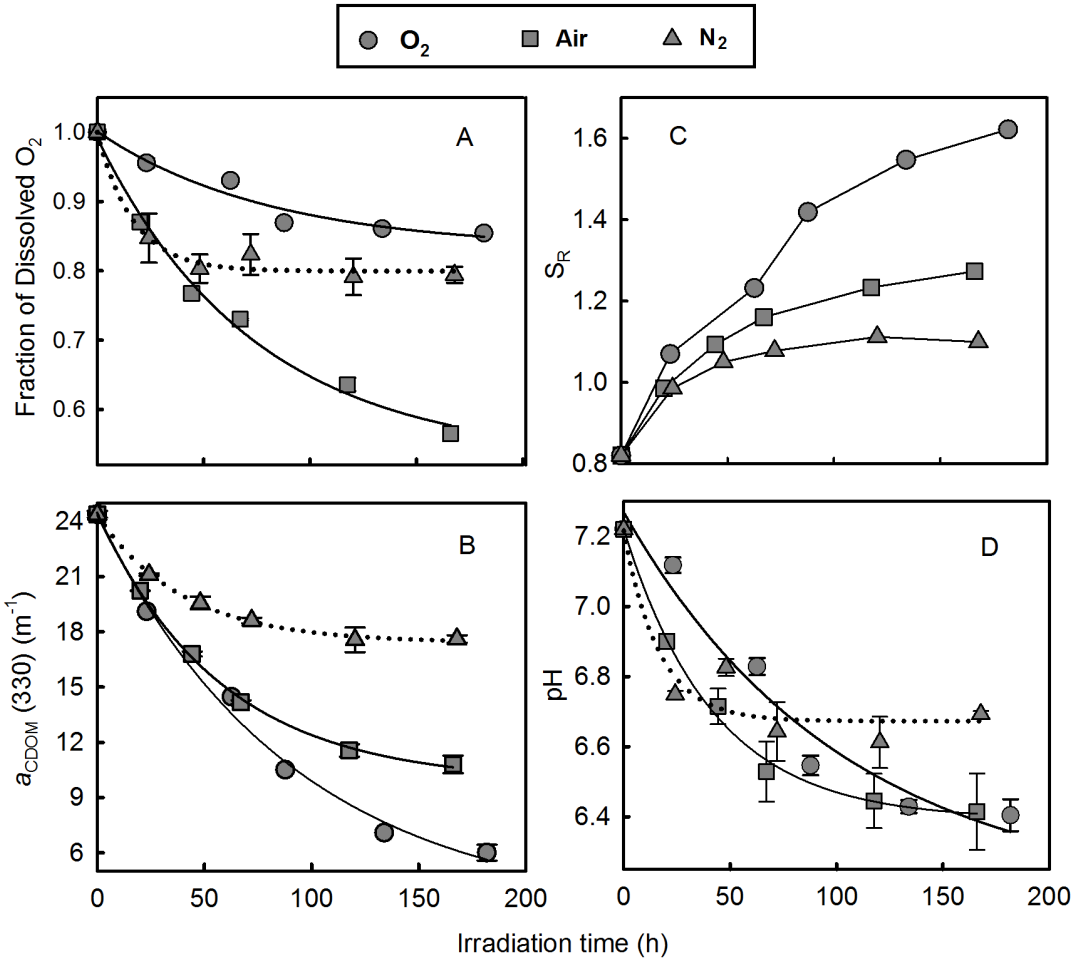

Fig. 3. Fraction of dissolved O_2 (A), $a_{CDOM}(330)$ (B), S_R (C), and pH (D) versus irradiation time.

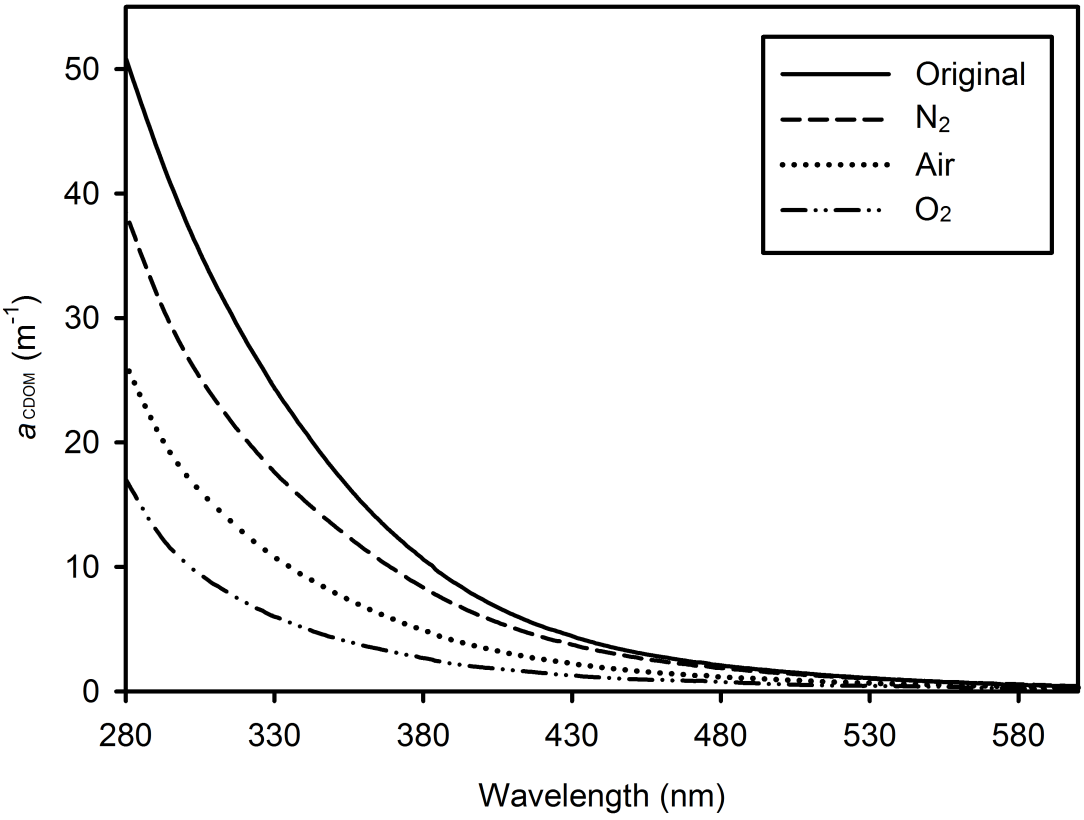

Fig. 4. Comparison of absorption spectra before and after full-spectrum irradiations.

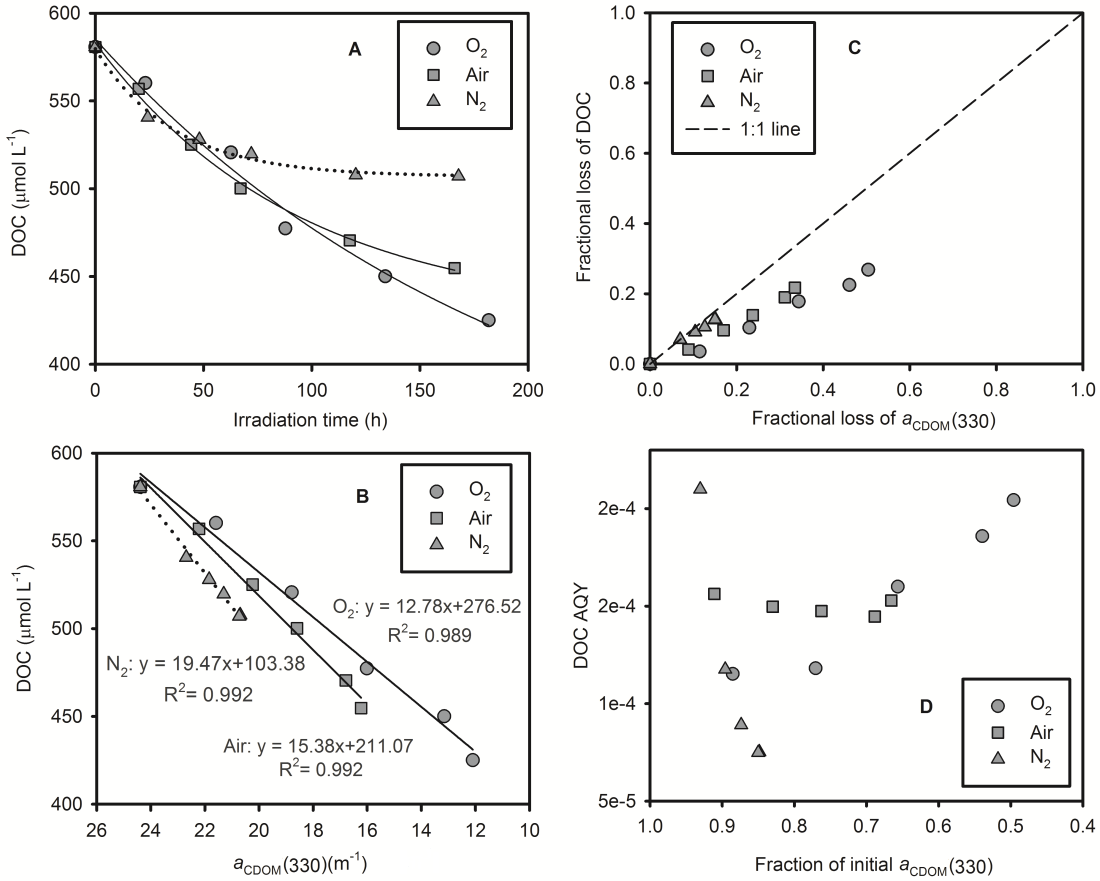

Fig. 5. [DOC] versus irradiation time (A) and $a_{CDOM}(330)$ (B), fractional loss of DOC versus fractional loss of $a_{CDOM}(330)$ (C), and AQY_{DOC} versus fraction of initial $a_{CDOM}(330)$ (D). Lines in panels A and B are best fits of the data. Fitted equations for panel A are presented in Table 1.

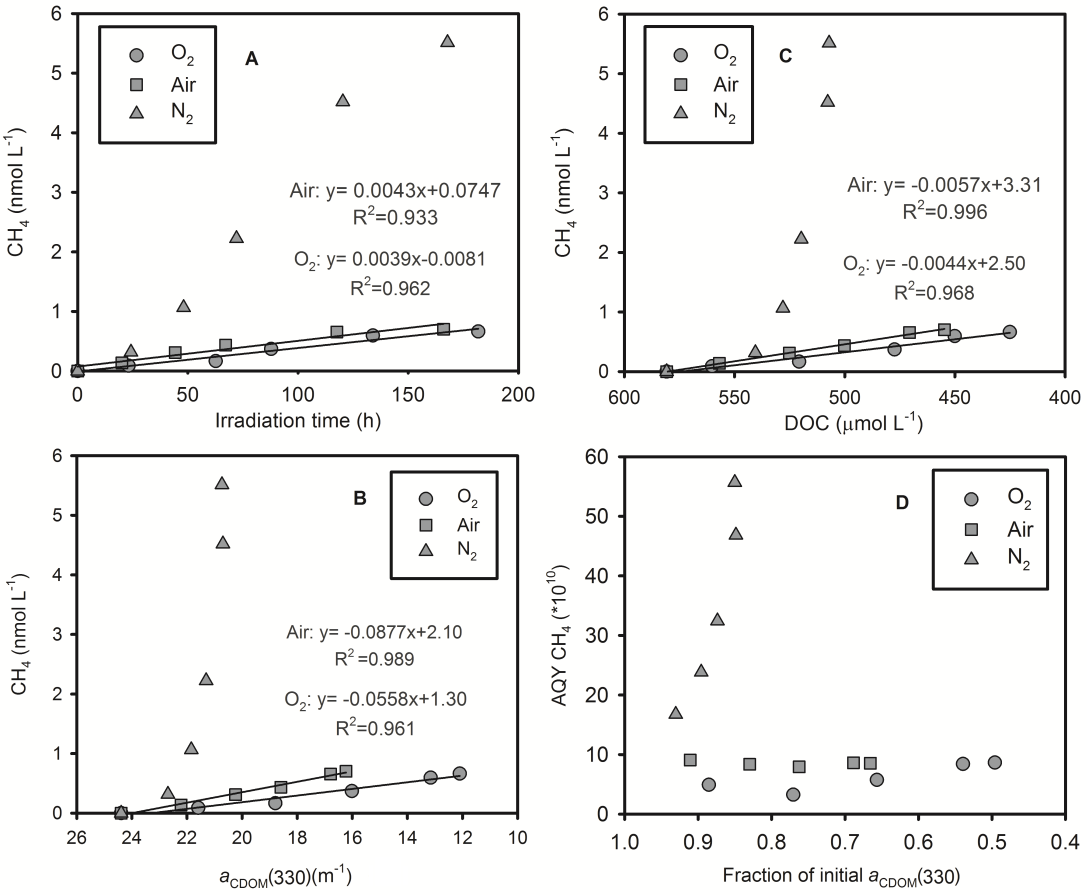

Fig. 6. [CH_4] versus irradiation time (A), $a_{CDOM}(330)$ (B) and [DOC] (C), and AQY_{CH4} versus fraction of initial $a_{CDOM}(330)$ (D). Lines in panels A, B and C are best fits of the data.

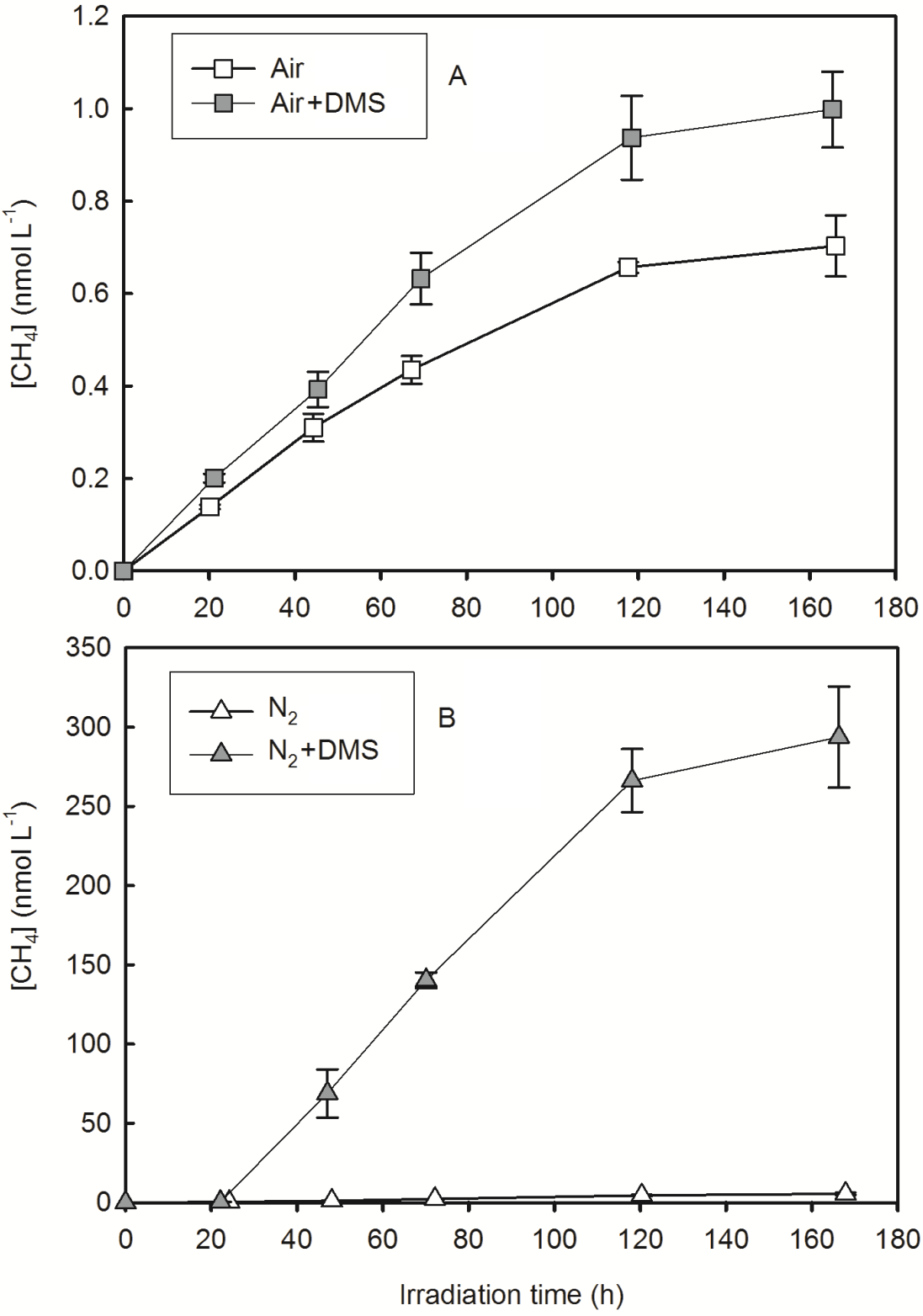

Fig. 7. Effect of DMS spiking (20 μmol L^{-1}) on CH_4 photoproduction in a time-series irradiation under air- and N_2-treatments (A & B).

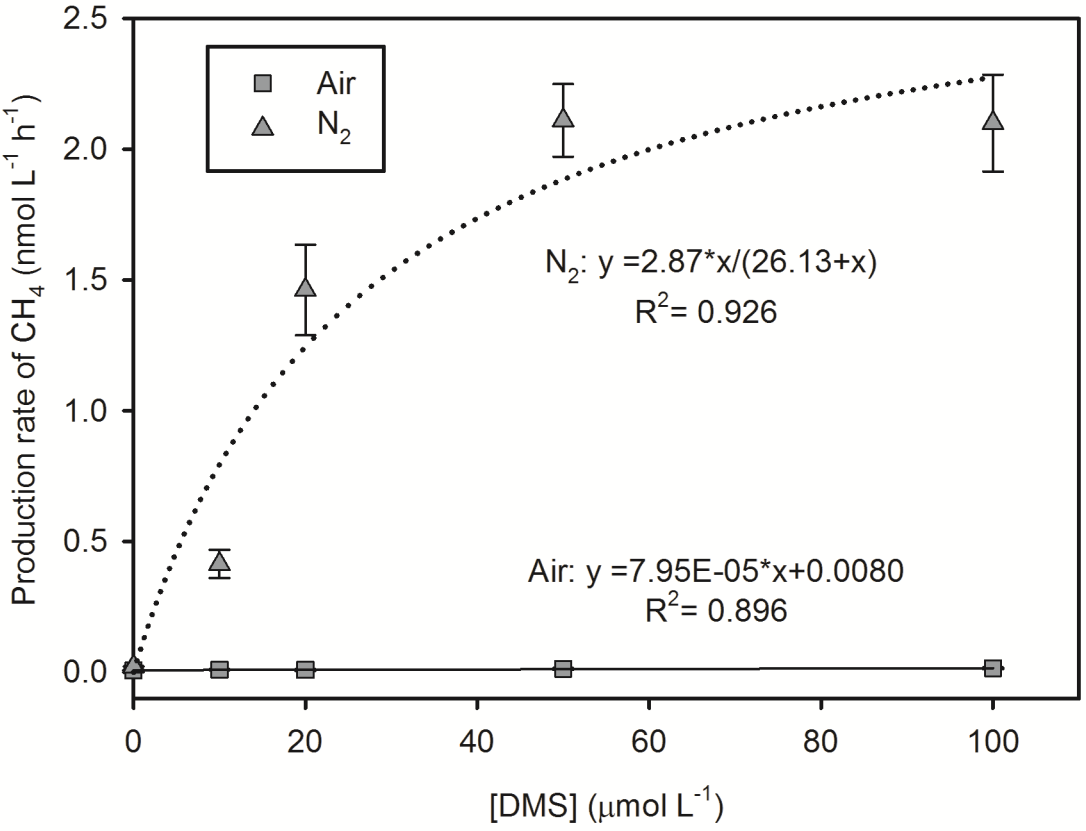

Fig. 8. Photoproduction rate of CH_4 as a function of added [DMS].